5-2021

Microstructural refinement of cement paste internally cured by polyacrylamide composite hydrogel particles containing silica fume and nanosilica

Baishakhi Bose

Cole R. Davis

Kendra Erk
Purdue University, erk@purdue.edu

Article

Microstructural Refinement of Cement Paste Internally Cured by Polyacrylamide Composite Hydrogel Particles Containing Silica Fume and Nanosilica

Baishakhi Bose, Cole R. Davis and Kendra A. Erk*
School of Materials Engineering, Purdue University, West Lafayette, IN 47907 USA
*Correspondence: erk@purdue.edu, 765-494-4118

Abstract:
Supplementary cementitious materials were incorporated into hydrogel-based internal curing agents to improve the hydration, microstructure, and ultimately strength of internally cured high-performance cement paste. Polyacrylamide composite hydrogel particles containing amorphous silica – either silica fume or nanosilica – and two different polymer network crosslink densities were synthesized and incorporated into cement paste. The presence of silica and low crosslink density increased the absorption capacity of the particles in pore solution. Micrographs of internally cured paste indicated a significant improvement in hydrogel-related void-filling ability and an increase in void size for low crosslink density particles containing silica. Compressive strength and electrical resistivity increased at later ages for paste samples containing particles with higher silica dosage. The relationship between extent of hydration, void size, and void-filling activity was found to strongly influence the paste's long-term strength and is thus an important structure-property relationship to consider when selecting hydrogels for internal curing purposes.

Keywords: microstructure (B); silica fume (D); cement paste (D); polymers (D); internal curing

1. Introduction

The growing demand for concrete with better quality in terms of strength and durability while ensuring low carbon footprint has led to the development of high-performance concrete (HPC). HPC,

however, is prone to self-desiccation and shrinkage [1], [2], due to the low water-to-cement (w/c) ratio used in its production. To mitigate the scarcity of water in HPC, superabsorbent polymer (SAP) particles have been successfully used in previous research as internal curing agents [3]–[7]. SAPs can absorb large amounts of water during mixing of concrete and release the water as the concrete ages, facilitating hydration reactions. Use of SAPs has been proven to be effective in preventing self-desiccation [5], mitigating autogenous shrinkage [4], [8]–[12], sealing cracks [13]–[15], improving resistance to freeze-thaw attack [16],[17], improving the microstructure [18] from the additional hydration, thereby enhancing strength and durability of the concrete.

The introduction of SAPs into concrete is not without challenges. The dosing and size of the hydrogel-based particles must be carefully monitored to ensure that the mechanical strength of the bulk concrete is not compromised by large voids left behind by the dehydrated SAPs. Furthermore, the rheological properties of fresh mortar are governed by the chemical structure of the SAPs [19]. The timing of water release is also of paramount importance: desorption during the acceleration period of the cement paste aids in mitigating autogenous shrinkage and improvement in hydration [20].

Additionally, SAPs are not chemically inert. SAPs used in cementitious systems are primarily composed of poly(acrylic acid-acrylamide) [19], [21], [22]. Multivalent cations – which are abundant in the alkaline pore solution of freshly mixed concrete – have been shown to induce rapid dehydration (deswelling) of swollen hydrogel particles [18],[20],[23],[24]. In particular, complete collapse of polymer networks comprised primarily of acrylic acid (sodium acrylate) has been observed [8], as the carboxylic acid groups in these networks become anionic in alkaline environments and are able to complex with free cations [25]. Thus, SAPs containing acrylic acid are prone to premature water release in cementitious environments, potentially causing an increase in effective w/c ratio and decreasing the compressive strength of mortar [26]. Desorption of acrylic acid-rich SAPs has been observed in previous studies to occur within few minutes in

free swelling experiments [8] and reduces the effectiveness of the internal curing if it occurs during the dormant period.

Considering the sensitivity of acrylic acid to pore solution composition, the present study focuses on acrylamide-based hydrogel particles which are not strongly ionized in alkaline environments and thus are expected to display more desirable, stable swelling behavior in cementitious mixtures. Acrylamide-rich SAPs have previously been shown to be more resistant to changes in pore solution chemistry [27] and have also displayed inorganic phase growth within the voids which remained in the cement microstructure after SAP dehydration [18][28]. This “void-filling” phenomenon was even more pronounced for hydrogel particles containing only acrylamide [29]. Also, a greater percentage of acrylamide in the hydrogel was observed to promote adhesion to the cement matrix, which further appeared to facilitate desorption of the hydrogel particles due to capillary effects [30], [31].

Supplementary cementitious materials (SCMs) have recently grown in popularity as a strategy to reduce the carbon footprint caused by the cement industry while improving the strength and durability of HPC. Both silica fume (SF) [32], [33] and nanosilica (NS) [34]–[36] have been used for partial replacement of cement or in conjunction with cement as binder material in cementitious systems. In addition to fostering pozzolanic reactions, NS also acts as a filler material to improve microstructure [37]. The high surface area of NS promotes nucleation of calcium silicate hydrate (C-S-H) [38], which presumably leads to higher compressive strengths. However, there are some issues when incorporating these fine-grained SCMs into cement-composites. For example, particles are subject to agglomeration at higher dosages and may reduce mixture workability [38]. Additionally, the fineness of the particles may create inhalation hazards during processing and exacerbate respiratory issues in workers, although amorphous silica has not been conclusively proven to cause pulmonary sicknesses [39].

Several research studies have been conducted previously in presence of both SAP particles and silica (in the form of NS or SF) to improve performance of internally cured cementitious systems

[40]–[44]. Mechanical strength of SAP-cured mortar containing NS was comparable to reference mortar without SAP [45]–[47]. Another study showed that inclusion of SAP reduced shrinkage when added to concrete containing NS, while maintaining slump [48]. Addition of SAP to SF-containing mixes showed that autogenous shrinkage was effectively reduced and more than half of the volume of SAP-related voids were filled with portlandite [49]. It is important to note that in these previous studies, SAP and silica were separately incorporated into the cementitious mixtures; as described here, the present study investigates the effects of directly combining SAP and silica.

A novel method of incorporating amorphous NS into poly(acrylic acid-acrylamide) hydrogel particles to form a "composite" hydrogel has already been reported by Erk and Krafcik *et al.* [50][51]. Cement paste internally cured with acrylamide-rich composite hydrogels particles displayed greater growth of hydration products in SAP-related voids compared with pastes containing conventional (silica-free) SAPs as well as those containing acrylic acid-rich composite hydrogel particles. Another study conducted by Davis *et al.* showed that the swelling capacity and the growth of products inside SAP-related voids can be enhanced by decreasing the crosslink density of the polyacrylamide particle [29]. Thus, polyacrylamide-silica composite hydrogel particles appear to have an advantage over conventional SAPs by promoting pozzolanic reactions in vicinity of the SAP-related voids while continuing to facilitate internal curing. Also, as the NS is physically confined within the polymer network during synthesis of the composite hydrogel, NS inhalation risks during concrete batching and casting are expected to be minimized.

The goal of the present study is to measure the effect of dosage and type of silica and the crosslink density of the polyacrylamide network on the performance of polyacrylamide composite hydrogel particles as internal curing agents. Two types of amorphous silica (SiO_2) were chosen for this study – NS and SF – keeping in mind the most common SCMs used in the concrete industry. Each different type of hydrogel was synthesized at two different crosslink densities. Figure 1 shows a schematic of the

polyacrylamide network with and without silica particles, with a relatively high and low density of crosslinks before and after hydration. The absorption behavior of composite hydrogel particles was characterized using gravimetric swelling tests. Experiments were then performed on cement paste internally cured by composite hydrogel particles to determine the impact on non-evaporable water content, density, porosity, inorganic phase development, and compressive strength.

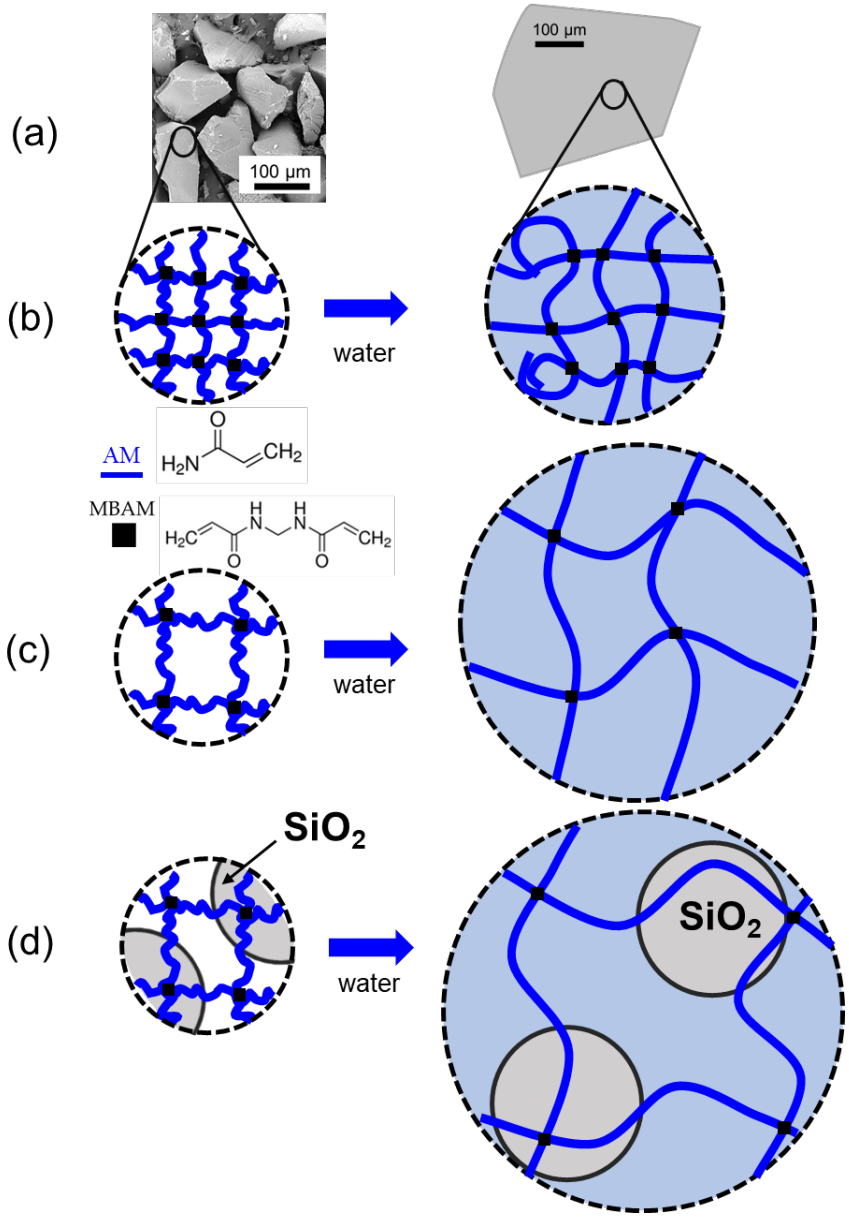

Figure 1: A schematic representations (not to scale) of the hydrogel particles in dry and hydrated state in (a) macroscale; (b) nanoscale at a high crosslink density without the presence of silica; (c)

nanoscale at a low crosslink density without the presence of silica; and (d) with silica particles confined within the network of a low crosslink density particle.

2. Material and Methods

2.1 Silica Characterization

Two sources of amorphous silicon dioxide (SiO_2; silica) were utilized in this study. Silica nanoparticles (NS) with a reported diameter of 60-70 nm were purchased from U.S. Research Nanomaterials, Inc. (Houston, TX). Silica fume (SF) with a reported diameter of 150 nm was purchased from Norchem, Inc. (Beverly, OH). X-ray diffraction (XRD) was performed on the as-received SF and NS silica particles using a Siemens D500 diffractometer (30 mA, 50 kV) at 0.02°/s scanning rate in (10–40)° 2θ range (Siemens AG, Germany). Samples were prepared by loosely packing the silica particles into a metal sample holder pressed to a paper surface in order to avoid preferential orientation of the particles.

A Zetasizer Nano ZS (Malvern Instruments, Malvern, United Kingdom) was used to measure the zeta potential of dilute suspensions of silica dispersed in Deionized (DI) water. For each type of silica, two samples were created at different values of pH, 7.1 ± 0.1 and 9.8 ± 0.1, through the progressive addition of a 2M NaOH solution and measured with an electronic pH meter. Measurements at pH > 10 were not possible with the existing Zetasizer configuration. Silica particles were added to the solution at a concentration of 0.1 wt.%, sonicated with a Branson Digital sonicator at 25% amplitude for 2 minutes, and allowed to equilibrate at 25°C for 6.5 hours prior to testing. Three measurements were performed for each sample and averaged to report the zeta potential.

2.2 *Hydrogel Synthesis*

Hydrogel particles were synthesized following the solution polymerization method. Acrylamide (AM, monomer), N,N'-methylenebisacrylamide (MBAM, crosslinker), sodium metabisulfate (NaS_2O_5), sodium persulfate (NaS_2O_8), were all

purchased from Sigma-Aldrich (St. Louis, MO) and used without further purification. Deionized (DI) water used for the synthesis of hydrogels was collected from a Barnstead Nanopure Infinity system (Barnstead Thermolyne Corporation, Ramsey, MN). DI water used had a resistivity of >18 Mohm cm.

Crosslinking solutions were prepared by adding 0.3 g of MBAM to 20 mL of DI water. Initiator solutions were prepared by adding 0.3g of NaS_2O_5 and NaS_2O_8 to 10 ml of DI water, separately (initiator dosage was fixed at 1% by monomer weight). Fresh batches of crosslinking and initiator solutions were prepared for each batch of hydrogel synthesis. The reagents used and their proportion in each variation of hydrogel are summarized in Table 1. Two dosages of silica and crosslinker were investigated: a silica dosage of 1 and 10% by weight of monomer and crosslinker dosage of 0.5 and 2% by weight of monomer. In Table 1, composite hydrogels are labelled as "X-Y-Z" to indicate composition, where "X" is either NS or SF, "Y" is the dosage of silica (1 or 10), and "Z" is the dosage of crosslinker (0.5 or 2).

Table 1: Hydrogel compositions.

Hydrogel	**AM (g)**	**Water (mL)**	**Crosslinking Solution (mL)**	**Silica (g)**
AM-2	3.0	7.0	4.0	-
SF-1-2	3.0	7.0	4.0	0.030
SF-10-2	3.0	7.0	4.0	0.300
NS-1-2	3.0	7.0	4.0	0.030
NS-10-2	3.0	7.0	4.0	0.300
AM-0.5	3.0	7.0	1.0	-
SF-10-0.5	3.0	7.0	1.0	0.300
NS-10-0.5	3.0	7.0	1.0	0.300

The hydrogel synthesis was adapted from Krafcik *et al*. [50]. To minimize the absorption of water on the silica, particles were placed inside 20 mL glass scintillation vials, covered with aluminum foil, and kept in a vacuum oven at 23°C for 8 hours. Particles were then stored in a desiccator prior to use. The required amount of water and silica (as per dosage requirement, see Table 1) were added to a centrifuge tube and ultrasonication was performed to disperse the particles. A Branson Digital sonicator equipped

with a tapered microtip for low volumes (3 mm tip for 1-10 mL, Sigma-Aldrich) was used to sonicate the suspensions at 35% amplitude for 2 minutes and then at 40% amplitude for 3 minutes.

The hydrogel synthesis reaction was conducted in 20 mL glass scintillation vials. The water-silica suspensions were added to the vials first. AM monomer and the prepared crosslinking (MBAM) solution in required amount (see Table 1) was added to the vials and stirred for 5 minutes. Then, 0.5 mL of each of the freshly prepared initiator solutions were added to the vial, and the vial was capped and placed in a temperature-controlled oil bath set at 60°C until gelation was observed (typically within 10 minutes). It is worth mentioning that following the current procedure for hydrogel synthesis, attempt to increase the dosage of silica beyond 10% by weight of monomer prevented gelation (sample-spanning percolation of the polymer network, [52]) from occurring.

Following gelation, the reaction product – a bulk hydrogel – was removed from the vial and immersed in DI water for 24 hours at 23°C to remove any unreacted reagents. The hydrogels containing silica differed in appearance compared with the silica-free hydrogels. Hydrogels containing NS were more opaque compared to pure AM hydrogels while hydrogels containing SF were shades of grey, with the intensity of grey increasing with SF dosage. TDS measurements of the DI "wash" water were nearly identical before and after hydrogel immersion. This, along with the variation in color of the synthesized hydrogels, provides evidence of the silica being physically confined in the polymer network even when hydrogels were swollen and immersed in fresh water. Also, no visible sedimentation of silica aggregates was observed in the synthesis vials or wash beakers.

2.3 Creation and Characterization of Hydrogel Particles

Bulk hydrogels were dried in an oven at 80 ± 1°C for 10 hours and then ground into a fine powder using an electric grinder and a mortar and pestle. Hydrogel particles were then sieved into different size fractions by vibrating a set of standard ASTM sieves on a mechanical vibrator table for 30 minutes at 1725 rpm. Particles retained on the sieves with mesh size of 45, 75, and 114 µm were added to a scintillation vial in equal weight proportions,

mixed, and then capped to form a representative sample of each hydrogel type with particle size ranging from 45 to 150 µm. To prevent any moisture uptake from the atmosphere, the vials of representative samples were kept sealed under laboratory conditions at 23°C, away from direct exposure to sunlight or moisture. This representative sample of hydrogel particle size was used for all the tests in this study except select compressive strength of cement paste using different sized hydrogels. Hydrogel particles were imaged using a NanoScience Instruments Phenom Desktop scanning electron microscope (Thermo Fisher Scientific, Waltham, MA), (uncoated sample, 15 kV). The synthesized hydrogel particles in their dry form along with the scanning electron micrograph of SF-10-2 are shown in Figure 2. Some silica particles are visible on Figure 2b in the form of bright white spots on the surface of the hydrogel particle.

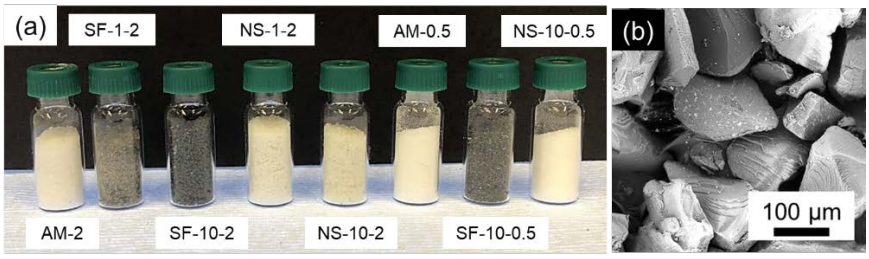

Figure 2: (a) Synthesized dry hydrogel particles. Each vial contains 1.10 ± 0.01 g. (b) Scanning electron micrograph of SF-10-2, showing the angular morphology of the hydrogel particles.

2.4 Gravimetric Swelling Tests of Hydrogel Particles

The tea-bag method [53],[54] was employed to quantify the absorption capacity of the hydrogel particles in both reverse osmosis (RO) water and pore solution. Previous researchers have used synthetic or extracted pore solution to characterize swelling behavior of SAPs [8], [55], [56]. SAP absorption capacity studied using tea-bag tests have been found to be an overestimation of the amount of water that would be absorbed when placed in cement mixes [57][58], however it serves as a simple, reproducible test to estimate the swelling capacity of SAPs.

Here, pore solution was prepared by adding tap water to cement at a water-to-cement ratio of 10 and stirring, covered, for 4 hours.

The solution was poured through a Büchner funnel under vacuum with a 589/3 Whatman filter paper (diameter of 150 mm) to remove the cement particles. The filtered solution was kept covered in a plastic container to minimize carbonation effects. Fresh pore solution was prepared for each batch of gravimetric swelling tests.

For both solutions (RO and pore solution), 200 mL of liquid was added to a beaker and a teabag was fully immersed into the solution for 30 seconds. The teabag was allowed to drip dry and then weighed to obtain the wet mass of the bag, m_{bag}. Then, 0.2 g of dry hydrogel particles (m_{dry}) were added to the wet teabag. The teabag was then immersed into the solution and removed at regular time intervals for weighing (m_{wet}). In the case of pore solution, the beakers were covered with aluminum foil in between measurements to minimize carbonation. Swelling tests were conducted in triplicate. The swelling ratio, Q (grams of absorbed fluid per grams of dry hydrogel particles), was calculated using the following formula:

$$Q = \frac{m_{wet} - m_{bag} - m_{dry}}{m_{dry}} \quad (1)$$

2.5 Creation and Characterization of Internally Cured Cement Paste

2.5.1 Batch Mixing of Cement Paste

Ordinary Type I Portland cement (ASTM C150) obtained from Buzzi Unicem (Greencastle, IN) was used. The properties of the cement from the manufacturer's mill certificate are reported in Table 2. Mixture proportions for the mixing of cement paste are given in Table 3. Tap water was used for mixing and the admixture used was Glenium 3030 NS full-range water reducer (WRA) supplied by BASF (Ludwigshafen, Germany). Hydrogel dosage (0.2% by weight of cement) and WRA amount were kept constant (see Table 3).

Five control samples (denoted as "C.XX" in Table 3) were investigated for the compressive strength study. The first three control samples, C.35, C.35-AM-2 and C.35-AM-0.5, have w/c

ratios of 0.35, the same w/c ratio that was used for all pastes internally cured with composite hydrogel particles. The other two controls, C.30 and C.40, were created to provide upper and lower bounds of comparison with the internally cured pastes. These bounds were chosen based on the maximum equilibrium absorption capacity that was observed in this study for NS-10-0.5 sample. Some researchers will add extra "curing" water to SAP-containing mixtures (e.g., 5%) to maintain mixture workability [24]. Here, no additional "curing" water was added to the mixture and given the relatively low absorption capacity of acrylamide-based SAPs observed at 24 hours compared with commercial SAPs, there was no detectible change in workability of mixtures with and without hydrogel particles.

Table 2: Cement properties.

Blaine Fineness	381 m^2/kg
Loss on Ignition	2.19 wt.%
SiO_2	19.58%
Al_2O_3	5.17%
Fe_2O_3	2.84%
CaO	63.78%
MgO	2.40%

Table 3: Mixture proportions for cement pastes (WRA in % by weight of cement).

Sample Name	Cement (g)	Water (g)	Hydrogel particles (g)	WRA (%)
C.35	100	35	--	0.70
C.35-AM-2	100	35	0.2	0.70
C.35-AM-0.5	100	35	0.2	0.70
C.30	100	30	--	0.70
C.40	100	40	--	0.70
SF-1-2	100	35	0.2 [a]	0.70
SF-10-2	100	35	0.2 [b]	0.70
NS-1-2	100	35	0.2 [a]	0.70
NS-10-2	100	35	0.2 [b]	0.70
SF-10-0.5	100	35	0.2 [b]	0.70
NS-10-0.5	100	35	0.2 [b]	0.70

[a] containing 0.0004% silica by weight of cement

[b] containing 0.004% silica by weight of cement

Dry cement and dry hydrogel particles (if applicable) were added to a mixing cup and hand mixed for 30 seconds. Water and WRA were added simultaneously, and the mixture was hand-mixed for 60 seconds, scraped from the sides of the container, allowed to rest for 30 seconds and then mixed for another 60 seconds before pouring into cylindrical molds each of 1" diameter and 2" height. The molds used for this study were developed by Davis *et al.*[29]. Molds were sealed and kept in an environmental chamber at 23 ± 0.1°C and 50% relative humidity for 24 hours. The paste samples were then demolded and stored in the environmental chamber (23 ± 0.1°C and 50% relative humidity) until testing. Samples utilized for electrical resistivity tests were placed in saturated lime water until testing after demolding. Care was taken to ensure that the level of saturated lime water remained constant for the duration of test period.

2.5.2 Density Measurements

Density measurements were conducted on cement paste samples to evaluate if the voids left behind by the hydrogel particles introduced significant porosity so as to affect bulk density. After the 7- and 28-day compressive strength tests, pieces from the paste sample were collected to conduct density measurements. The specimens (3 for each cement paste sample) were dried in an oven for 3 days at 110 ± 5 °C until constant mass was obtained. The specimens were immersed in DI water at temperature of 23 ± 1°C for 24 ± 4 hours. Specimens were then dried on a large piece of absorbent cloth and the mass of each specimen was measured (in saturated surface dry condition, (*B*)). The specimens were again immersed in water and its apparent mass measured, (*C*). The specimens were dried in the oven for 24 hours at 110 ± 5 °C and the oven dried mass was measured (*A*). The oven dried (OD) specific gravity and the absorption capacity (in percentage) in terms of *A*, *B* and *C* are given by the following equations:

$$Oven\ dried\ specific\ gravity = \frac{A}{(B-C)} \qquad (2)$$

$$Absorption\ (\%) = \frac{(B-A)}{A}\ x\ 100 \qquad (3)$$

2.5.3 Non-Evaporable Water Content Measurements

Internal curing water held by SAPs may increase the degree of hydration [59]. This test is a commonly used method to provide an indication of the hydration of cementitious materials [60]. A small piece from the 28-day cement paste sample (cast and stored in the manner described in Section 2.5.1) was immersed in isopropanol for 24 hours, ground and sieved using a sieve with mesh size of 250 µm. About 3 g of the ground cement paste was dried for 24 h in an oven at 105°C. Then, the samples were ignited in a muffle furnace at 1050°C for 3 h. The mass of the samples was measured using a balance with a 0.0001 g resolution and was used to calculate the non-evaporable water content using the following equation:

$$W_n = \frac{m_{105} - m_{1050}}{m_{1050}} - LOI \qquad (4)$$

where W_n is the non-evaporable water content (g/g cement paste), m_{105} is the dry mass (g), m_{1050} is the ignited mass (g), and LOI is the loss on ignition of cement, which is 2.19% according to the mill certificate provided by the manufacturer. The test was run in triplicate and average values were reported.

2.5.4 Backscattered Electron Microscopy

Cement paste prepared using the method described in Section 2.5.1 were used for electron microscopy imaging. Microstructure analysis was performed on 3 days old cement paste. Cured cylinders were immersed in isopropanol for 24 hours to stop hydration, cut into manageable pieces with a diamond saw, vacuum dried for 72 hours at (23 ± 5) °C, and then vacuum impregnated with epoxy. The epoxy coated cement paste samples were then dried at (60 ± 5) °C for 48 hours. Then, a fresh section of each epoxy coated sample was exposed by cutting with a diamond saw and polished. The samples were then carbon coated and imaged using a NanoScience Instruments Phenom Desktop SEM. At least 30 random hydrogel particles' voids were imaged for further microstructural analysis using ImageJ to quantify the portions of the hydrogel particles' voids filled with some product of hydration. Details regarding the procedure implemented to

calculate area fraction of the hydrogel void filled with hydration products can be found in the supplementary material (Figure S1). The largest diameter for 30 voids within select paste samples was also measured to compare the hydrogel-related void size between different cement paste samples. Figure 3 illustrates the maximum diameter calculation process from a micrograph of a hydrogel void that is labeled with all the relevant features: original dimension of the hydrogel at the time of set, open void space, dehydrated hydrogel, and hydration product growth.

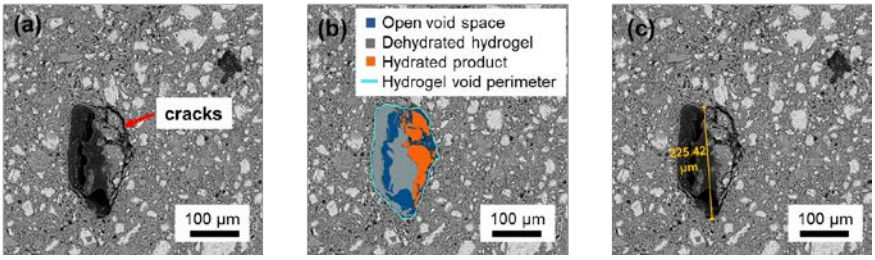

Figure 3: Micrograph of cement paste with hydrogel particle void. (a) Microstructure features within the local vicinity of the void clearly indicated the dimensions of the original swollen hydrogel particles, including visible cracks marked by the arrow. (b) Open void space, layers of dehydrated hydrogel and hydration product growth/deposit inside the void are highlighted along with the perimeter of the original swollen hydrogel particle at the time of set. (c) Line indicates the measured maximum diameter of the hydrogel particle.

2.5.5 Compressive Strength Measurements

Compressive strength tests were conducted on cement paste samples aged 3, 7, and 28 days using an Insight 820.300-SL machine with a load capacity of 300 kN (MTS Systems Corp., Eden Prairie, MN) at a constant strain rate of 1 mm/min. For each sample, three specimens were tested and the average compressive strength along with the standard deviation were calculated.

2.5.6 Thermogravimetric Analysis

Cement paste samples were used to quantify content of calcium hydroxide (CH) in 7- and 28-day samples by thermogravimetric analysis (TGA). Paste samples were taken out of the environmental

chamber at the specified days, hydration stopped by immersing in isopropanol for 24 hours and then ground into powder using a mortar and pestle. Care was taken to ensure the powder used for TGA analysis did not originate from the surface of the cylindrical paste sample to eliminate any potential effects of moisture condensation. The powder was sieved through No. 200 (75 µm) sieve and then dried in a vacuum oven at 23°C for 3 days until constant mass was obtained. A small sample of powder (15 to 25 mg in size) was used for TGA measurements using a 2050 Thermogravimetric Analyzer manufactured by TA Instruments (New Castle, DE) with platinum crucibles. Analysis was performed in a nitrogen gas atmosphere, with a temperature range of 23 °C to 1000 °C at a heating rate of 10 °C/min.

2.5.7 Electrical Resistivity Tests

The electrical resistivity of cementitious materials provides an indirect indication of porosity. It is a non-destructive means of investigating microstructural characteristics which in turn can aid in understanding the uptake and transportation of ions as the paste ages [61]. Cement paste samples were removed from the environmental chamber at specified days and the resistance of the samples was measured following procedure described by Spragg *et al.*[62] . The sponges were wetted in a freshly prepared saturated calcium hydroxide solution prior to each measurement, and the resistance of the top and bottom sponge was accounted for.

A separate study of the control samples (without any hydrogels) left in a controlled temperature environment without any curing water and another set in lime water was performed to ensure that there is no significant difference in electrical resistivity of samples if submerged in saturated lime water.

3. Results and Discussion

3.1 Silica Characterization Results

As shown in Figure 4, the XRD patterns indicated that both NS and SF are highly amorphous as the overall intensity of the signal was extremely low with a broad reflex, centered at about 22°. For

SF, a peak at 2θ ~ 35.5° was obtained due to the presence of silica carbide [63]. Crystalline silica would have given a pattern with two high-intensity peaks about the 2θ at 20.8° and 26.6°, respectively [64].

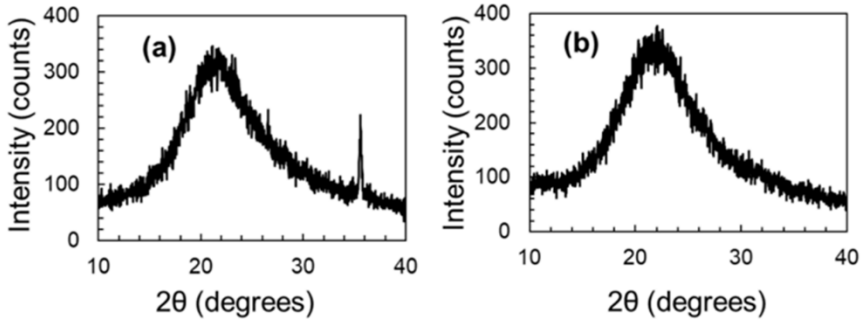

Figure 4: XRD pattern of the (a) silica fume (SF) (b) nanosilica (NS) used in this study.

The zeta potential measurements are given in Table 4. These results suggest that the amorphous silica particles have a negative surface charge due to the dissociation of terminal silanol groups and subsequent formation of surface hydroxyl (-OH) groups [65]. Also, the zeta potential values indicated that both forms of silica will be stable at the highly alkaline pH that is usually common in cementitious mixtures as aqueous dispersions with zeta potentials less than -30mV are considered to be stable [66].

Table 4: Zeta potential measurements of SF and NS.

Form of silica	pH	Zeta Potential (mV)
Silica Fume	7.1 ± 0.1	- 28.6 ± 0.7
(SF)	9.8 ± 0.1	- 41.3 ± 0.6
Nanosilica	7.1 ± 0.1	- 26.1 ± 2.4
(NS)	9.8 ± 0.1	- 41.6 ± 1.4

3.2 Hydrogel Absorption Results

Figure 5 shows the swelling capacities of hydrogel particle samples in RO water and pore solution. At a constant crosslink density of 2%, compared with pure (silica-free) AM particles, the addition of NS resulted in greater absorption in RO water, which at equilibrium (24 hours) increased by 19% and 55% for NS dosages of 1% and 10%, respectively. To a lesser extent, addition of SF

also increased the equilibrium absorption by 2% and 20% for SF dosages of 1% and 10%, respectively. Additionally, the decrease of crosslink density increased the swelling capacity by 110% for the pure (silica-free) AM particles, and similar trends were also observed for the silica-containing particles. For instance, a 80% increase in equilibrium swelling capacity of NS-10-0.5 was observed compared with NS-10-2. As expected, absorption capacities for each hydrogel sample were reduced in pore solution (Figure 5b), as the naturally occurring ions in pore solution reduced the osmotic driving force for water absorption [25]. It is important to note that no residues of silica particles were observed in the beakers after the swelling tests; *i.e.*, the NS and SF particles remained physically confined within the hydrogel particles even at maximum particle swelling.

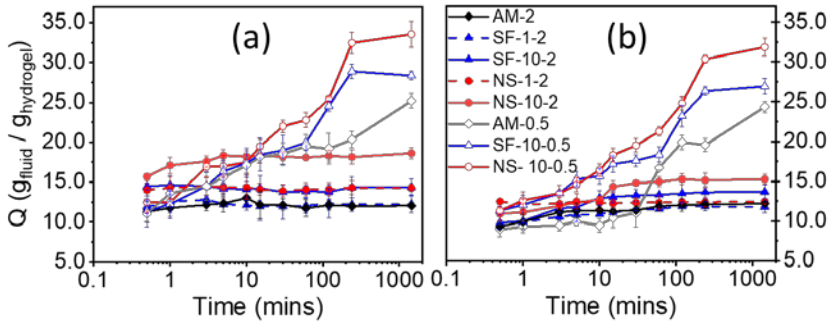

Figure 5: Swelling capacity of hydrogel particle samples as a function of immersion time in (a) RO water and (b) pore solution.

As seen in Figure 5, the NS-10-0.5 hydrogel particles, with lower crosslink density and containing NS, displayed the greatest absorption capacity in both RO water and pore solution. Two factors contributed to this behavior. First, reducing the crosslink density of the hydrogel particles effectively doubled their measured absorption capacity. This is well-known behavior in polymer physics [52], illustrated in Figure 1, as the presence of chemical crosslinks in a polymer network reduces the overall flexibility (degrees of freedom) of the polymer molecules and thus hinders volumetric expansion. Consistent with past work by Davis *et al*. [29], the greater network restrictions and reduced absorption due to crosslinks manifest as large increases in the particles' compressive, shear, and elastic moduli [29]. Second, zeta potential measurements (Table 4) indicated the likelihood of water

adsorption directly on to the silica particles driven by hydrogen bonding and dipole interactions of water molecules with surface hydroxyl groups [67]. As the silica particles were physically confined in the polymer network, such surface adsorption would manifest globally as an increase in absorption capacity. This idea is consistent with the greater increase in swelling observed for NS-containing hydrogel particles compared with SF, as the smaller NS particles displayed greater total surface area for water adsorption.

3.3 Density Measurement Results

The oven dried specific gravity (OD) and the absorption capacity of the cement pastes samples are reported in Figure 6. A slight increase in specific gravity and consequent decrease in absorption capacity of the cement pastes were observed with age. This was expected as over time, the cement paste hydrated and porosity decreased; hence, the density increased and the absorption capacity subsequently decreased. Interestingly, the addition any hydrogel particles – high or low crosslink density, containing NS or SF – did not significantly change the density of the paste samples compared with the control paste (C.35), indicating that the hydrogel-related voids did not significantly affect the bulk density of the paste samples at the chosen conventional dosage of 0.2 % hydrogel particles by weight of cement.

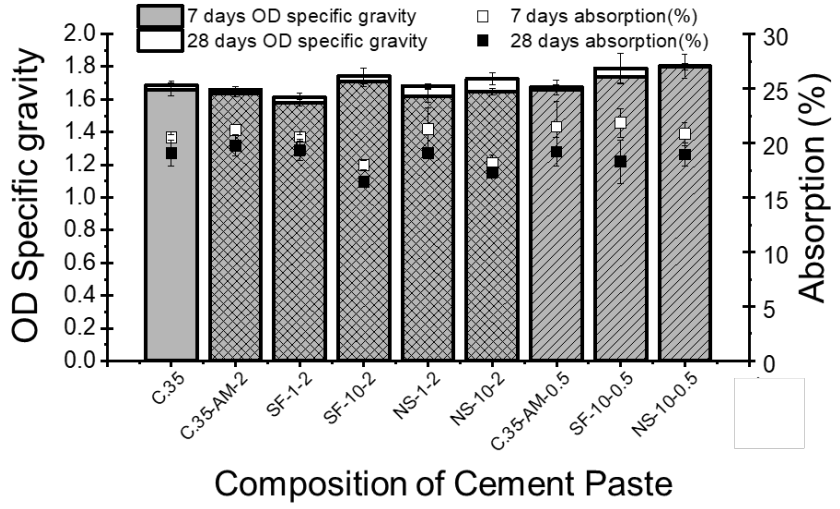

Figure 6: Oven dry (OD) specific gravity and absorption capacity of cement paste samples at 7 and 28 days. For clarity, hatched bars represent samples containing low crosslink density hydrogel

particles and cross-hatched bars represent samples containing high crosslink density hydrogel particles.

3.4 Non-Evaporable Water Content Results

The non-evaporable water content (W_n) at 28 days is shown in Figure 7. It was evident that the addition of hydrogel particles increased the hydration of the cement paste samples, which is in agreement with previous research performed on cement paste containing hydrogel particles [60]. Also, for the high crosslink density particles, an improved degree of hydration for paste containing composite hydrogel particles compared to paste samples containing silica-free hydrogels. No significant improvement of hydration was observed when comparing paste containing hydrogel particles with low crosslink density.

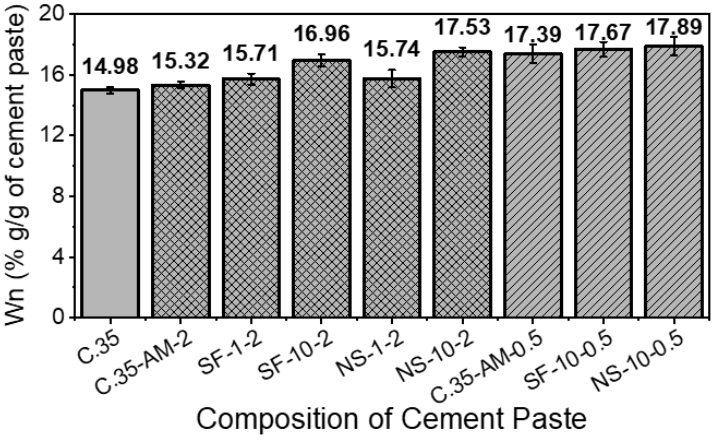

Figure 7: Non-evaporable water content (W_n) of the cement pastes at 28 days. For clarity, hatched bars represent samples containing low crosslink density hydrogel particles and cross-hatched bars represent samples containing high crosslink density hydrogel particles.

3.4 Cement Paste Microstructure

Scanning electron micrographs of internally cured cement pastes are shown in Figures 8 and 9 for high and low crosslink density hydrogel particles, respectively. For each sample, the sizes of the

hydrogel-related voids and the amounts of hydration product observed within the voids were measured and are described below to ultimately determine the effects of hydrogel particle composition – crosslink density and the presence of silica – on the cement paste microstructure.

The size of the hydrogel-related voids in the cement microstructure is an important parameter to estimate for each hydrogel particle composition as the presence of voids beyond a critical size will reduce cement strength. Additionally, hydrogel particle swelling capacity results from the free swelling experiments (Figure 5) cannot be directly applied to estimate void sizes in the microstructure. This is because during mixing and placement of cement, the hydrogel particles will likely experience physical confinement from the surrounding cement solids which can hinder the volumetric expansion of the hydrogel particles and ultimately reduce their capacity for fluid absorption.

To estimate the size of the hydrogel-related voids within the cement microstructure, the maximum diameter was measured for 30 randomly selected voids in each sample. Histograms of all measurements are available in supplementary material (Figure S2). Table 5 reports the average values to allow for relative comparisons to be made between different hydrogel particle compositions. While some quantitative information was lost when comparing average size values instead of complete size distributions, these averages were treated here as rough estimates of particle sizes due to the measurement challenges described in the following paragraph.

Table 5: Average maximum length of SAP-related voids from cement paste microstructure analysis.

Sample	Average maximum length of void (μm)
C.35-AM-2	212
SF-10-2	236
NS-10-2	239
C.35-AM-0.5	225
SF-10-0.5	290
NS-10-0.5	355

683 Example diameter measurements are provided in Figure S3 to
684 illustrate that the maximum diameters sometimes included regions
685 filled with hydration product, which was believed to form
686 during/after particle dehydration. As such, these measured
687 diameters provided a rough estimate of the size of the swollen
688 hydrogel particles at the cement setting time. In some images (e.g.,
689 Figure 8b; Figure 9b, d, and f), microstructure features within the
690 local vicinity of the void clearly indicated the dimensions of the
691 original swollen hydrogel particles, including visible cracks, open
692 void space, layers of dehydrated hydrogel, poorly consolidated
693 hydration product (also see Figure 3). However, in other images
694 (e.g., Figure 8d and f), such features were less visible when the
695 hydrogel-related voids contained significant growth of hydration
696 product, partially obscuring the original dimensions of the swollen
697 hydrogel particles. In these cases (< 9% of all analyzed images),
698 maximum diameter was determined by marking off the visible
699 edges of the hydrogel-related voids and then measuring the
700 diameter in several directions to obtain the maximum diameter (see
701 labeled image in supplementary material Figure S3, for more
702 details).
703
704 Despite these measurement challenges, some significant trends
705 were observed from Table 5. Most notable was the relatively
706 smaller swollen sizes displayed by the high crosslink density
707 particles compared with the low crosslink density particles. In the
708 free swelling experiments reported in Figure 5, the high crosslink
709 density particles only swelled to approximately half the capacity of
710 the low crosslink density particles after 24 hours, an expected
711 outcome due to the network restrictions imparted by the chemical
712 crosslinks. In the cement pastes, however, the differences in
713 swollen particle size reported in Table 5 were not as great due in
714 part to the confinement of the swelling particles by the surrounding
715 cement solids. This trend was also observed during a previous
716 study conducted by Erk and coworkers on cement paste internally
717 cured with spherical PAM [29]; for more details, see histograms in
718 supplementary material, Figure S4. Increases in swollen particle
719 sizes were observed when silica was present in the hydrogel
720 particles, again consistent with free swelling results in Figure 5.
721 For the high crosslink density particles containing silica, a small
722 increase in swollen particle size was observed (e.g., 13% increase

in size from C.35-AM-2 to NS-10-2) while greater increases were observed for low crosslink density particles containing silica (e.g., 58% increase in size from C.35-AM-0.5 to NS-10-0.5).

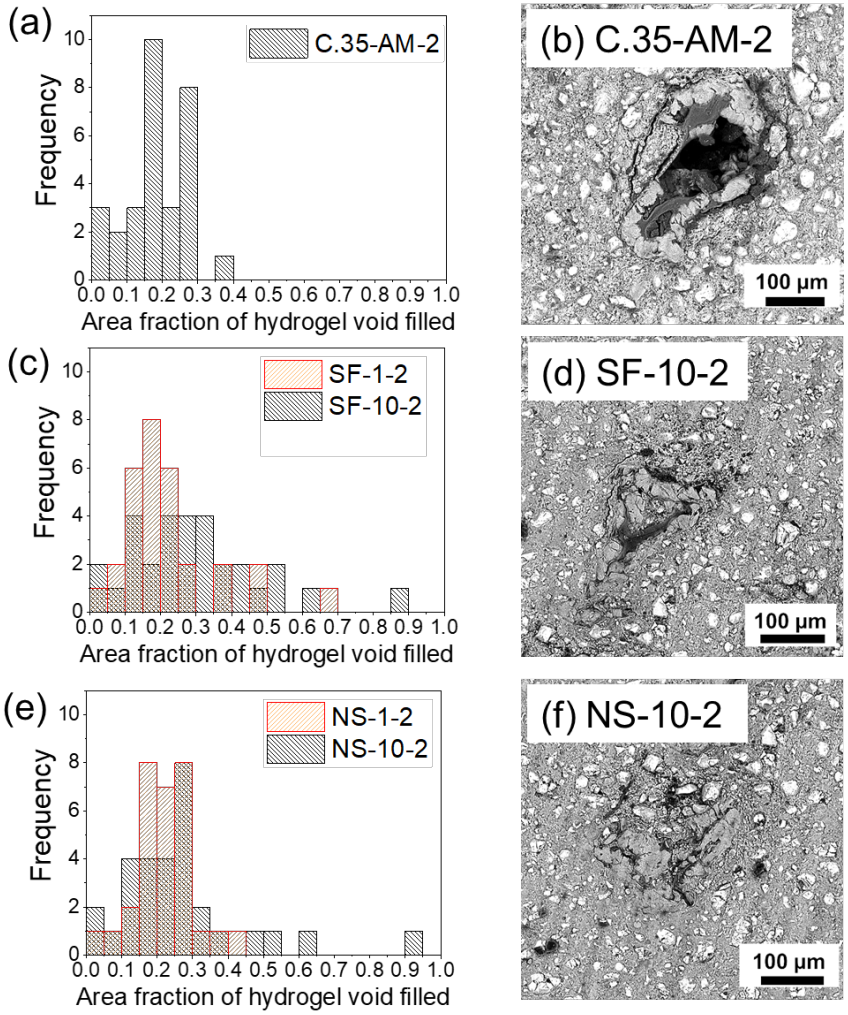

Figure 8: Microstructure analysis of pastes cured with high crosslink density hydrogel particles. (a) (c) and (e) Area of hydrogel particle voids filled with hydration products as a function of cement paste composition. Micrographs (3-day cured) of hydrogel particle voids in cement paste internally cured with (b) C.35-AM-2 with 35% of the void filled, (d) SF-10-2 with 89% of the void filled, and (f) NS-10-2 with 93% of the void filled.

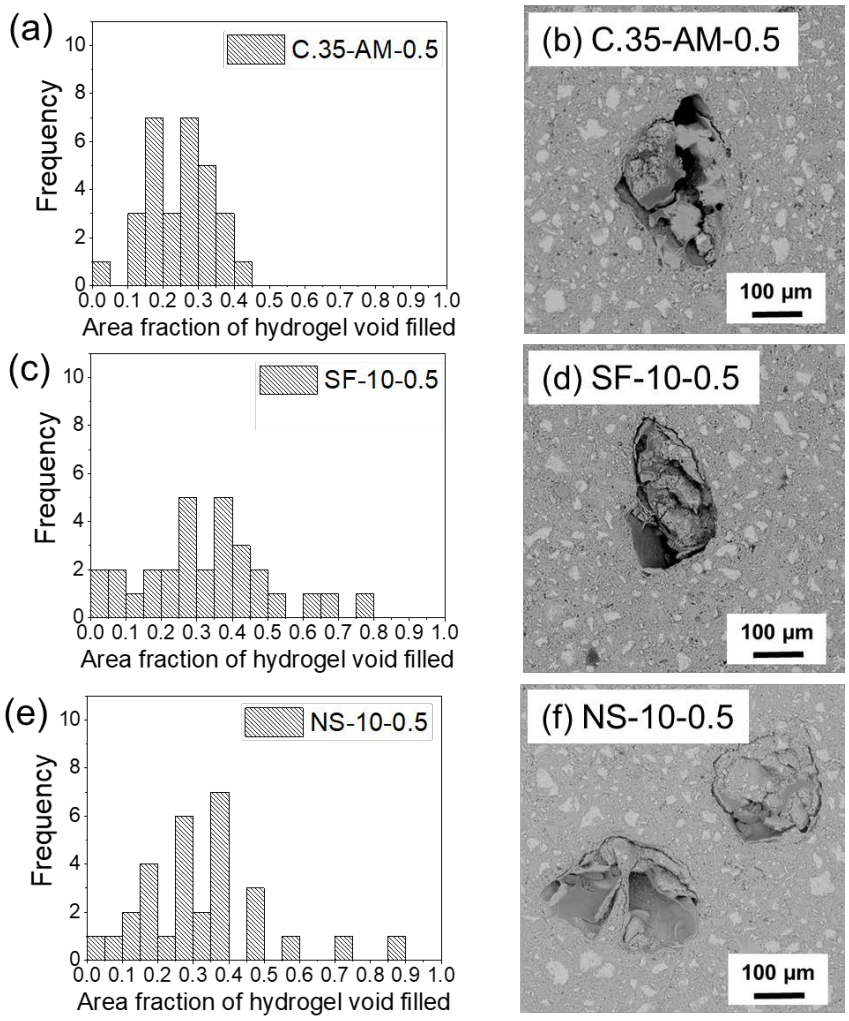

Figure 9: Microstructure analysis of pastes cured with low crosslink density hydrogel particles. (a) (c) and (e) Area of hydrogel particle voids filled with hydration products as a function of cement paste composition. Micrographs (3-day cured) of hydrogel particle voids in cement paste internally cured with (b) C.35-AM-0.5 with 40% of the void filled, (d) SF-10-0.5 with 80% of the void filled, and (f) NS-10-0.5 with 89% of the upper-right hand corner void filled.

As seen in the micrographs in Figures 8 and 9, one of the most striking features of the cement microstructures was the observed "filling" of the hydrogel-related voids with hydration product. Based on elemental analysis conducted in a prior study (see Figure S5), the hydration products are believed to be mostly CH with some amount of intermixed C-S-H.

To determine how the hydrogel particle composition affected the observed void-filling, the amounts (by area fraction) of hydration product observed within the hydrogel-related voids were quantified for each internally cured paste. Details of these measurements, including representative images, are provided in supporting information (Figure S1). Of the 30 hydrogel-related voids that were analyzed for paste containing high crosslink density particles (see histograms in Figure 8), the following numbers of voids were more than 30% filled: 1 void in C.35-AM-2; 5 voids in SF-1-2 and 13 voids in SF-10-2; 3 voids in NS-1-2 and 7 voids in NS-10-2. By comparison, of the 30 hydrogel voids analyzed for paste containing low crosslink density particles (see Figure 9), the following numbers of voids were more than 30% filled: 9 voids in C.35-AM-0.5; 16 voids in SF-10-0.5; and 15 voids in NS-10-0.5. Thus, more voids resulting from low crosslink density hydrogel particles containing silica were filled with hydration products compared to voids resulting from high crosslink density particles.

The greater filling of hydrogel-related voids in SF-10-2 and NS-10-2 samples was in good agreement with the increased amount of non-evaporable water observed in Figure 7. In particular, the SF-10-2 composite hydrogel particles appeared to have the greatest impact on the microstructure of the cement paste, potentially indicating that desorption and reaction rates may depend on silica form. Increased non-evaporable water content for NS-10-0.5 when compared to NS-10-2 was also observed which is consistent with the larger amount of filled hydrogel voids in NS-10-0.5.

The differences in void-filling ability observed in Figures 8 and 9 are most likely due to the different physical and chemical structures of the hydrogel particles, including the crosslink density and the presence of silica. The following paragraphs describe the hydrogel structure-property relationships that are hypothesized to directly impact the development of the cement microstructure.

The differences in absorption capacity (Figure 5) of the high and low crosslink density hydrogel particles were significant and important to consider when analyzing the internally cured paste microstructures. The significantly higher swelling capacity of the low crosslink density particles likely caused the hydrogels to retain

more water in the paste mixture. In turn, greater amounts of water may have facilitated more hydration product growth inside the voids during early stages of hydration. It was also expected to take longer to fully expel the absorbed water; hence, this additional water present for longer time durations might have facilitated growth of more products in and around the hydrogel-related voids. Additionally, it is noteworthy that the high-swelling low crosslink density hydrogel particles formed larger sized voids on average compared with the voids resulting from the low-swelling high crosslink hydrogels (see Table 5). Hence, the void-filling "activity" in the vicinity of the low crosslink density hydrogel particles appeared to be much greater than in the vicinity of the high crosslink particles, ultimately resulting in more total void space filled by hydration product in pastes cured with the low crosslink density hydrogel particles.

Besides dictating absorption capacity, the nanostructure of the hydrogel's internal polymer network may have played additional roles in the formation of hydration product. In particular, as illustrated in Figure 1, the high crosslink density hydrogels have higher polymer concentration and thus smaller mesh size (pore size) compared with the low crosslink density hydrogels. Inspired by existing hydrogel-based crystallization studies [68], the high crosslink density, small mesh size hydrogel particles were expected to more strongly hinder the nucleation and growth of hydration product within the hydrogel, by a combination of the following factors. First, the supersaturation threshold probably increased for the nucleation of inorganic phases including CH and C-S-H. This is supported by a study that found higher supersaturation levels are required for crystallization of calcium carbonate from solutions confined within gelatin-based hydrogels with smaller mesh size [69]. Second, the growth rate of the hydration products might have been significantly reduced due to slower diffusion of ions throughout the smaller mesh size of the hydrogel particle. As reported by Lopez-Bengaza *et al*.,[70] and others [71], hindrance of ion diffusion in agarose hydrogels with small mesh size resulted in slower growth of calcium carbonate. Third, the smaller mesh size might have physically confined the growing inorganic phases, thereby limiting the product's overall size and morphology, especially as the latter is typically dictated

by preferred crystallographic growth orientations. To summarize, chemical crystallization studies have found that mass transport in hydrogel-based materials is relatively slow and controlled because the mobility of ions in the solution is restricted by the polymer network and supersaturation concentrations can be more difficult to achieve. Ultimately, these changes in transport and chemical activity can slow the overall rate of crystallization and change the size and morphology of the resulting products. In the present work, such changes likely contributed to the reduced void-filling that was observed in pastes cured with the high crosslink density, small mesh size hydrogel particles.

In addition to crosslink density, the presence of silica within the hydrogel particles directly impacted the cement microstructure. For both the high and low crosslink density hydrogel particles, silica resulted in increased void-filling as illustrated in Figures 8 and 9. Thus, silica appeared to have increased the formation of hydrated product in the hydrogel-related void. This result was most likely due to silica acting as a filler material [37] in addition to fostering pozzolanic reactions. Furthermore, the high surface area of NS may have promoted nucleation of C-S-H over the surface [38]. The presence of silica inside the composite hydrogels along with the unrestricted space for nucleation and growth provided by the deswollen hydrogel void was also expected to contribute towards enhancement of hydration product growth.

Lastly, when considering the impact of the silica-containing hydrogels on the internally cured pastes, it is important to note that the relatively small dosage of the silica in the system did not result in detectible increases in global pozzolanic activity (results and details will be discussed in Section 3.6). In a previous study with spherical hydrogel particles, it was relatively straight-forward to distinguish CH growth by its typical morphology (Figure S5) and confirm with EDX measurements [29]. However, for the present study with irregular shaped hydrogel particles, the growth observed in the hydrogel-related voids was more complex and likely composed of CH intermixed with C-S-H. As such, EDX measurements were likely to be inaccurate and not performed.

3.5 Compressive Strength Results

The changes in compressive strength of the cement paste samples at various ages are shown in Figure 10, including the results for three hydrogel-free control samples, C.30, C.35, and C.40, which have w/c ratios of 0.30, 0.35, and 0.40, respectively (Figure 10a). The results for cement pastes containing high and low crosslink density hydrogel particles are shown in Figure 10b and 10c, respectively. After 28 days of curing, increases in strength beyond all control samples were observed for pastes containing high crosslink density hydrogel particles with the highest dosage of silica, i.e. SF-10-2 and NS-10-2 in Figure 10b. In comparison, the 28-day compressive strength values for pastes containing low crosslink density hydrogels were significantly reduced (Figure 10c).

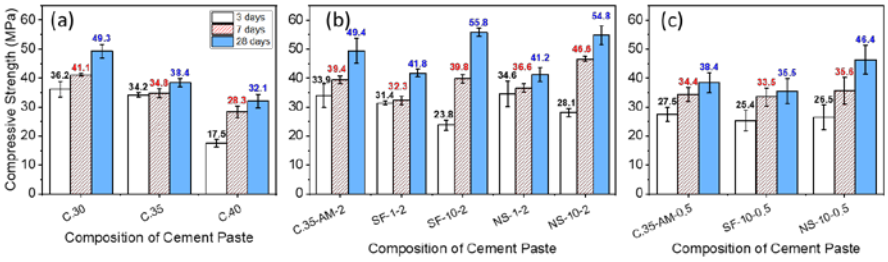

Figure 10: Compressive strength of cement pastes at various ages. (a) Control pastes at different w/c ratios without hydrogel particles; (b) pastes internally cured with high crosslink density hydrogel particles; and (c) pastes internally cured with low crosslink density hydrogel particles.

Reduced early-age (3 days) strength was observed for almost all paste samples containing composite hydrogel particles compared with the respective control pastes containing silica-free particles, i.e. C.35-AM-2 in Figure 10b and C.35-AM-0.5 in Figure 10c. Among internally cured samples, pastes containing hydrogels with the highest dosage of silica fume (SF-10-2) had the lowest early-age strength. Interestingly, the most significant gains in strength over the 28-day period were observed for pastes containing SF-10-2 (+135%) and NS-10-2 (+95%) when compared to the control paste C.35-AM-2 (+46%).

Reductions in early-age strength may be explained by considering the desorption behavior of the different hydrogel particles. As shown in Figure 10, the 3 days strength of paste containing composite hydrogel particles was reduced compared to silica-free hydrogel particles. This reduction could indicate that that the composite hydrogel particles were desorbing more fluid at earlier ages compared with the silica-free hydrogel particles, leading to a cement matrix that has a local w/c ratio greater than 0.35 and thus reduced strength. This idea is perhaps consistent with other published results[72], showing that the presence of SF in OPC-SCM systems increased the desorption rate of SAP hydrogel particles; as SF typically creates a finer pore structure, the authors suggested that the presence of SF facilitates hydrogel desorption by increasing the capillary pressure of the matrix. Here, the silica confined within the composite hydrogel was not released from the particle; however, the silica may still increase the local capillary pressure, leading to accelerated desorption at early ages.

It is important to note that fluid desorption from the hydrogel particles into the cement matrix was not directly observed or measured in this study. The results from the 24-hr free "*ex situ*" swelling experiments shown in Figure 5 did not display any signatures of fluid desorption. Additionally, swelling tests conducted for up to 3 days did not show any significant change in swelling capacity compared with the 24-hr absorption values in Figure 5 (see Figure S6 in supplementary material). While *ex situ* swelling tests are useful to determine the equilibrium absorption of a particular SAP formulation, it is well known that these tests are not completely accurate representations of the environment that a SAP particle experiences when confined in a cement matrix [25]. Specifically, in *ex situ* swelling tests, like Figure 5, there are no significant chemical or physical driving forces that evolve over time to encourage fluid desorption from the hydrogel particles. For example, Montanari, *et al.* [27] recently showed that the sorption behavior of SAP was dependent on the concentration of ions in the pore solution which of course changes over time during hydration.

To better understand the relationship between longer term (28 days) compressive strength and microstructure, Table 6 summarizes the relative changes of hydration product growth, void

size, and compressive strength for select hydrogel compositions. From Table 6, for silica-free hydrogels, a decrease in crosslink density corresponded to a 33% increase in void-filling, a small (6%) increase in void size, and a 22% decrease in 28 days compressive strength. The negative correlation between void-filling and compressive strength was unexpected as it was assumed that the compressive strength of the paste would increase if more of the SAP-related voids were filled with hydrated product. This unexpected observation may instead indicate that at the relatively low hydrogel dosages used in this study, any strength gains which resulted from SAP-related void-filling were local and did not contribute towards the global compressive strength.

Table 6: Impact of crosslink density decrease on hydration product growth in hydrogel-related voids, void size and 28 days compressive strength.

Comparison Samples	Average area of hydration product in hydrogel voids	Average diameter of hydrogel-related void	Compressive Strength of cement paste
C.35-AM-2 to C.35-AM-0.5	33% ↑	6% ↑	22% ↓
SF-10-2 to SF-10-0.5	12% ↑	23% ↑	36% ↓
NS-10-2 to NS-10-0.5	28% ↑	49% ↑	15% ↓

For the SF-containing hydrogel samples compared in Table 6, a decrease in crosslink density corresponded to a moderate increase (12%) in void-filling and a dramatic 36% decrease in 28 days compressive strength. So again, the expected benefits of void-filling were not observed at the global scale. In this case, the dramatic strength reduction between the samples have resulted from the substantial increase in size (23%) of the hydrogel-related voids, which could increase the likelihood for crack initiation and propagation during compression testing and result in failure at reduced loads. For the NS-containing hydrogel samples compared in Table 6, a decrease in crosslink density corresponded to a 28% increase in void-filling, a large increase (49%) in void size, and a moderate decrease (15%) in 28 days compressive strength. So,

despite the fact that the low crosslinked NS-containing hydrogels created relatively large voids in the cement paste, the compressive strength was not as dramatically reduced like for the SF samples, perhaps due to the increased void-filling abilities of these NS-containing hydrogels.

Overall, the comparisons illustrated in Table 6 and the results in Figure 10 clearly indicate that the compressive strength of cement paste containing hydrogel particles was dependent on the crosslink density of the particles, as the higher-swelling low crosslink density hydrogel particles resulted in reduced long term compressive strengths. Table 6 also shows that there was not one dominant feature of the microstructure that completely explained the strength reductions, as both a hydrogel's void-filling ability as well as its total void size appeared to play important roles.

In one final experimental attempt to better understand the relationship between hydrogel-related microstructure features and paste compressive strength, another set of compressive strength tests were conducted on paste samples containing dried and sieved low crosslink density hydrogels with different particle sizes (Figure 11). Samples denoted in Figure 11 as "-75" contained low crosslink density particles with dry sizes of 45-75 μm; samples denoted as "-114" contained low crosslink density particles with dry sizes of 75-114 μm. Paste samples containing composite silica-containing hydrogels with larger particle size resulted in small but significant strength reductions at all ages (3, 7, 28 days). For instance, compared to the NS-10-0.5-75 sample, there was a 16% reduction in 28 days strength for NS-10-0.5-114. Such reductions were expected as larger particles will swell to greater dimensions in the cement paste and result in larger hydrogel-related voids. Although hydration product growth in these voids might offset some of the loss in strength, larger voids will lead to reduced overall strength.

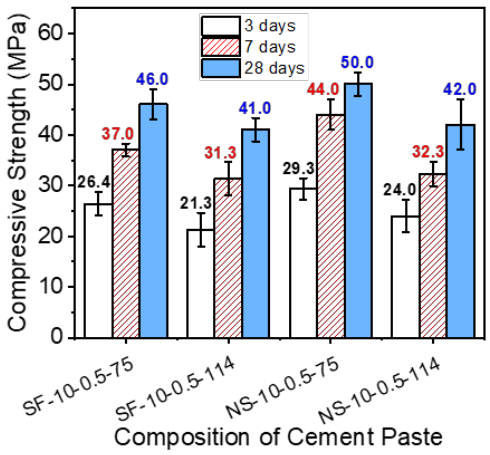

Figure 11: Compressive strength of cement pastes at various ages internally cured with 0.5% crosslinked hydrogel particles of different size ranges: "-75" denotes dry particles within 45-75 µm and "-114" denotes dry particles within 75-114 µm.

To summarize, considering the comparisons in Table 6 and data in Figures 10 and 11, increased hydrogel-related void size in the cement paste microstructure due to either larger hydrogel particles or hydrogel particles with lower crosslink density (and thus greater swelling) resulted in compressive strength reductions. However, as illustrated by the NS-containing hydrogels, these void-size-dependent strength reductions were at least partially off-set by the growth of hydrated product within the voids.

3.6 Phase Analysis

The CH content in the cement paste samples at two hydration ages is shown in Figure 12. As hydration proceeded, the amount of CH increased in the samples. CH content further increased with silica dosage in the hydrogel; for example at 28 days, a 14% increase in CH within the NS-10-2 paste sample was observed compared to the internally cured control (C.35-AM-2) sample.

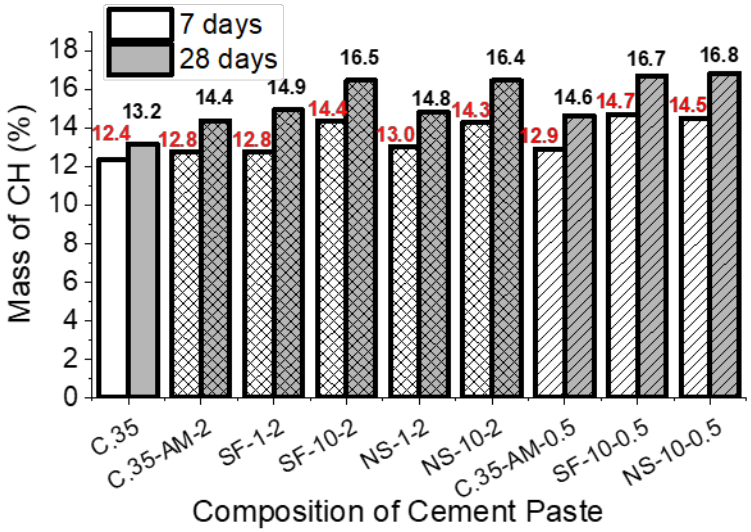

Figure 12: Calcium hydroxide content (%) of cement paste at 7 and 28 days. For clarity, cross-hatched bars represent samples containing high crosslink density hydrogel particles and hatched bars represent samples containing low crosslink density hydrogel particles.

In systems containing SCMs, the conversion of CH to C-S-H should decrease the CH content when compared to samples without any SCM. Here, the observed increases in CH in Figure 12 in samples containing composite hydrogels indicate that the presence of silica in the hydrogel particles did not impact the global CH content inside the paste matrix. While unexpected, this was not a surprising outcome as even at the highest dosage of silica in the hydrogel particles (10 wt.% of monomer), silica was less than 0.005 wt.% of the cement used in fresh paste mixture. The silica concentration in a single swollen SF-10-2 or NS-10-2 particle was estimated to be approximately 0.5-1.5 vol.% based on starting reagent concentrations in Table 1, average silica and dry hydrogel particle size, and swelling dimensions from micrographs. To put these dosages into context, typical NS dosages in conventional OPC-SCM mixtures range from 0.2 to 12 wt.% of cement [73]. Thus, the dosage of silica in the paste mixtures of this study was most likely insufficient to decrease global CH content as C-S-H is created, as measured by TGA. Instead, the measured increase in CH in Figure 12 was consistent with the results from the non-evaporable water measurements (Figure 7), indicating that

pastes internally cured with composite hydrogel particles had increased degree of hydrations.

No significant changes in CH content were observed in Figure 12 for samples cured with low crosslink density hydrogels compared with high crosslink density hydrogels, despite the increases in void-filling observed in pastes containing low crosslink density particles (see Table 6). For instance, in Figure 12, the increase in CH content was 15% in NS-10-0.5 sample, when compared to C.35-AM-0.5. As aforementioned, the increase in CH content for NS-10-2 sample was 14%, when compared to C.35-AM-2. This observation again supports the idea that at these relatively low dosages of hydrogel particles in cement pastes, any local microstructural or compositional changes related to the hydrogel particles may be difficult to quantify directly using global characterization techniques, like macroscale compression testing or TGA.

3.7 Results from Electrical Resistivity Tests

Resistivity is related to the volume and connectivity of pores inside the paste samples, and conductivity is primarily due to pore solution [62]. In general, as paste hydrates over time, pore volume decreases, causing a corresponding increase in resistivity. As shown in Figure 13, there was a prominent increase in resistivity for paste samples containing composite silica-containing high crosslinked hydrogel particles after 21 days when compared to all other paste sample.

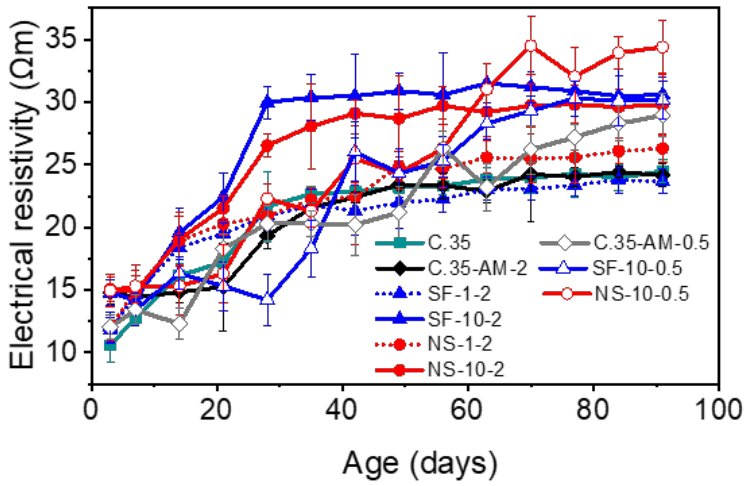

Figure 13: Variation of electrical resistivity of cement paste samples with the age of the sample.

Similar trends have been seen in another study with SAPs [61] which suggested that the electrical resistivity of cementitious systems containing SAP was dependent on two competing factors: increased amount of macrovoids (including SAP-related voids) and densification of the pore structure in the vicinity of SAP-related voids as a result of enhanced water replenishment. The results in Figure 13 suggest that the dominant factor for pastes internally cured with high crosslink density hydrogels was the latter – an increased degree of hydration due to the presence of hydrogel particles. The SF-10-0.5 did not show any marked improvement when compared to the SF-10-2 samples, which might be because the larger macrovoids played a more important role in the resistivity of the paste containing lower crosslinked hydrogels.

The increase in resistivity of samples containing SF-10-0.5 and NS-10-0.5 composite hydrogel particles when compared to other control samples suggest that the dosage and size range of composite hydrogel particles was insufficient to cause a connected pore structure that would increase conductivity of ions. This was confirmed by the images of the hydrogel-related voids (Figures 8 and 9) showing that the internally cured cement paste did not have an interconnected pore system. Growth of hydration product inside the hydrogel-related voids decreases the porosity and hence causes a gradual increase in resistivity over time. Similar decrease in

porosity in the micro- and mesopore range have been observed in cement paste containing SAP by previous researchers [74].

3.8 Comparisons with Prior Work

Compared to previous investigations [50] of the swelling behavior of poly(acrylic acid-acrylamide) hydrogel particles with and without NS, the polyacrylamide composite hydrogel particles studied here displayed lower absorption capacity in RO water and pore solution and were less sensitive to fluid composition, displaying similar equilibrium swelling values in both environments. In the previous investigation, hydrogel particles containing a high concentration of acrylic acid also displayed relatively fast desorption (rapid deswelling) during immersion in pore solution due to the interactions of the anionic segments in the polymer network with naturally occurring cations in the pore solution. As expected, the acrylamide-based particles studied herein were much less sensitive to pore solution composition due to their low anionicity and thus did not display any significant desorption behavior even after 3 days of immersion in pore solution.

The acrylamide-based composite hydrogel particles studied here displayed much greater void-filling ability after 3 days of hydration compared with particles containing a high concentration of acrylic acid with and without NS [50], [75]. However, even in acrylic acid-based hydrogel particles, addition of silica resulted in a measurable increase in the formation of hydration product within the hydrogel-related voids [50], consistent with present results. Significant void-filling behavior was also observed in pastes containing suspension polymerized (spherical) polyacrylamide hydrogel particles not containing silica [29]. In this prior work, hydrogel particles that had low crosslink density (0.5 wt.% MBAM) and thus higher absorption capacity also displayed greater void-filling ability compared to particles with higher crosslink density (2 wt.% MBAM) and lower absorption capacity which was consistent with the present study results.

Together, these comparisons with prior work indicate that the presence of silica in the hydrogel particles as well as the organic

chemistry of the polymer network jointly impact the void-filling ability of these particles and thus corresponding paste properties. Specifically, pozzolanic reactions and corresponding strength gains appear to be more extensive for pastes containing composite hydrogel particles that retain fluid in the presence of silica for a greater length of time, even if the overall absorption capacity of these particles is relatively low. That is, compared to high-capacity, fast-desorbing hydrogel particles composed of acrylic acid, acrylamide-based composite hydrogel particles swell less in pore solution but have increased void-filling abilities such that incorporation of these low-swelling yet highly retentive particles in cement allows for microstructural refinement and gains in compressive strength by pozzolanic reactions to be realized.

4. Conclusions

Polyacrylamide composite hydrogel particles containing silica led to better hydration of internally cured cement paste compared to silica-free hydrogel particles. The main findings were as follows:

- Equilibrium free swelling capacities of composite hydrogels with low crosslink density and higher silica dosage were greatest among the hydrogels studied. This was attributed to the silica facilitating water absorption and the lower crosslink density allowing the polymer molecules more degrees of freedom, leading to increased swelling.
- For pastes including composite hydrogel particles with higher dosage of silica and higher crosslink density, the compressive strength and electrical resistivity increased substantially at later ages compared to hydrogel-free pastes and pastes containing silica-free hydrogel particles, also consistent with the increase in non-evaporable water content.
- The microstructure analysis of internally cured cement paste showed that some of the hydrogel-related voids were filled with hydration products after 3 days. This “void-filling” phenomenon was more extensive in pastes cured with composite hydrogel particles with low crosslink density and higher dosage of silica. These samples also displayed the largest average diameter of hydrogel-related voids.

- The size of the hydrogel-related void appeared to play a more important role in determining compressive strength at later ages than the local microstructure refinement due to void-filling. However, results indicated that strength reductions due to larger void sizes may be at least partially off-set by the growth of hydrated product within the voids, which was enhanced by the presence of silica in the hydrogel particles.
- Overall, for the acrylamide-based hydrogels that were synthesized in this study, the selection of silica type – nanosilica or silica fume – did not play as strong a role in defining hydrogel absorption behavior (and thus internal curing performance) as the magnitude of crosslink density within the polymer network.

From this study, it is clear that the relationship between extent of hydration, void size, and void-filling activity will strongly influence long-term strength and is thus an important structure-property relationship to consider when selecting SAPs for internal curing purposes. From a practical perspective, the incorporation of silica within the hydrogel's polymer network allows for supplementary cementitious materials to be incorporated in a novel manner without undue health hazards associated with nanomaterials. And a greater dosage of silica may be used in the future to enhance pozzolanic reactions and further increase the quality of the concrete internally cured with composite hydrogel particles. This research also found that the crosslink density of polyacrylamide networks can be specifically manipulated to ensure that acrylamide-rich SAPs achieve sufficient swelling capacities and can thus be effective internal curing agents.

Acknowledgments

The authors would like to thank the Lyles School of Civil Engineering at Purdue University for allowing the use of the Charles Pankow Concrete Materials Laboratory, Dr. Jan Olek for his insights into analysis of the TGA data, and Dr. Raikhan Tokpatayeva for her assistance with the XRD measurements.

Conflicts of interest

The authors have no conflicts of interest to declare.

Funding

This work was funded by the National Science Foundation, CAREER award CMMI #1454360. The sponsors of research had no involvement in study design, collection, analysis and interpretation of data, writing of the report, and in the decision to submit the article for publication.

Author Contributions

Baishakhi Bose: Conceptualization, Data curation, Investigation, Visualization, Original draft preparation, Editing draft
Cole R. Davis: Investigation, Data curation, Reviewing draft
Kendra A. Erk: Funding acquisition, Conceptualization, Reviewing and editing draft

References

[1] W. J. Weiss, W. Yang, and S. P. Shah, “Shrinkage Cracking of Restrained Concrete Slabs,” *J. Eng. Mech.*, vol. 124, no. 7, pp. 765–774, 1998.

[2] P. Lura, O. M. Jensen, and J. Weiss, “Cracking in cement paste induced by autogenous shrinkage,” *Mater. Struct.*, vol. 42, no. 8, pp. 1089–1099, 2009.

[3] H. Beushausen, M. Gillmer, and M. Alexander, “The influence of superabsorbent polymers on strength and durability properties of blended cement mortars,” *Cem. Concr. Compos.*, vol. 52, pp. 73–80, 2014.

[4] O. M. Jensen and P. F. Hansen, “Water-entrained cement-based materials : II. Experimental observations,” *Cem. Concr. Res.*, vol. 32, no. 6, pp. 973–978, 2002.

[5] O. M. Jensen and P. F. Hansen, “Water-entrained cement-based materials: I. Principles and theoretical background,” *Cem. Concr. Res.*, vol. 31, no. 4, pp. 647–654, 2001.

[6] S. Oh and Y. C. Choi, “Superabsorbent polymers as internal curing agents in alkali activated slag mortars,” *Constr. Build. Mater.*, vol. 159, pp. 1–8, 2018.

[7] O. M. Jensen and P. Lura, “Techniques and materials for internal water curing of concrete,” *Mater. Struct.*, vol. 39, no. 9, pp. 817–825, 2006.

[8] M. J. Krafcik and K. A. Erk, “Characterization of superabsorbent poly(sodium-acrylate acrylamide) hydrogels and influence of chemical structure on internally cured

mortar," *Mater. Struct.*, vol. 49, no. 11, pp. 4765–4778, 2016. doi:10.1617/s11527-016-0823-7

[9] D. Snoeck, O. M. Jensen, and N. De Belie, "The influence of superabsorbent polymers on the autogenous shrinkage properties of cement pastes with supplementary cementitious materials," *Cem. Concr. Res.*, vol. 74, pp. 59–67, 2015.

[10] L. Montanari, P. Suraneni, and W. J. Weiss, "Accounting for Water Stored in Superabsorbent Polymers in Increasing the Degree of Hydration and Reducing the Shrinkage of Internally Cured Cementitious Mixtures," *Adv. Civ. Eng. Mater.*, vol. 6, no. 1, pp. 583–599, 2017.

[11] V. Mechtcherine *et al.*, "Effect of internal curing by using superabsorbent polymers (SAP) on autogenous shrinkage and other properties of a high-performance fine-grained concrete: results of a RILEM round-robin test," *Mater. Struct.*, vol. 47, no. 3, pp. 541–562, 2014.

[12] L. De Meyst, J. Kheir, J. R. Tenório Filho, K. Van Tittelboom, and N. De Belie, "The Use of Superabsorbent Polymers in High Performance Concrete to Mitigate Autogenous Shrinkage in a Large-Scale Demonstrator," *Sustainability*, vol. 12, no. 11, p. 4741, 2020.

[13] A. Mignon *et al.*, "pH-responsive superabsorbent polymers: A pathway to self-healing of mortar," *React. Funct. Polym.*, vol. 93, pp. 68–76, 2015.

[14] D. Snoeck, S. Steuperaert, K. Van Tittelboom, P. Dubruel, and N. De Belie, "Visualization of water penetration in cementitious materials with superabsorbent polymers by means of neutron radiography," *Cem. Concr. Res.*, vol. 42, no. 8, pp. 1113–1121, 2012.

[15] H. X. D. Lee, H. S. Wong, and N. R. Buenfeld, "Self-sealing of cracks in concrete using superabsorbent polymers," *Cem. Concr. Res.*, vol. 79, pp. 194–208, 2016.

[16] V. Mechtcherine, C. Schrofl, M. Reichardt, A. J. Klemm, and K. H. Khayat, "Recommendations of RILEM TC 260-RSC for using superabsorbent polymers (SAP) for improving freeze–thaw resistance of cement-based materials," *Mater. Struct.*, vol. 52, no. 75, 2019.

[17] V. Mechtcherine *et al.*, "Effect of superabsorbent polymers (SAP) on the freeze–thaw resistance of concrete: results of a RILEM interlaboratory study," *Mater. Struct.*, vol. 50, no. 1, p. 14, 2017.

[18] M. Krafcik, N. Macke, and K. A. Erk, "Improved Concrete Materials with Hydrogel-Based Internal Curing Agents," *Gels*, vol. 3, no. 4, pp. 46–64, 2017. doi: 10.3390/gels3040046.

[19] V. Mechtcherine, E. Secrieru, and C. Schröfl, “Effect of superabsorbent polymers (SAPs) on rheological properties of fresh cement-based mortars — Development of yield stress and plastic viscosity over time,” *Cem. Concr. Res.*, vol. 67, pp. 52–65, 2015.

[20] C. Schroefl, V. Mechtcherine, P. Vontobel, J. Hovind, and E. Lehmann, “Sorption kinetics of superabsorbent polymers (SAPs) in fresh Portland cement-based pastes visualized and quantified by neutron radiography and correlated to the progress of cement hydration,” *Cem. Concr. Res.*, vol. 75, pp. 1–13, 2015.

[21] L. P. Esteves, “Superabsorbent polymers: On their interaction with water and pore fluid,” *Cem. Concr. Compos.*, vol. 33, no. 7, pp. 717–724, 2011.

[22] Q. Zhu, C. W. Barney, and K. A. Erk, “Effect of ionic crosslinking on the swelling and mechanical response of model superabsorbent polymer hydrogels for internally cured concrete,” *Mater. Struct.*, vol. 48, no. 7, pp. 2261–2276, 2015. doi: 10.1617/s11527-014-0308-5.

[23] S.H. Kang, S.G. Hong, and J. Moon, “Importance of monovalent ions on water retention capacity of superabsorbent polymer in cement-based solutions,” *Cem. Concr. Compos.*, vol. 88, pp. 64–72, 2018.

[24] P. Zhong, M. Wyrzykowski, N. Toropovs, L. Li, J. Liu, and P. Lura, “Internal curing with superabsorbent polymers of different chemical structures,” *Cem. Concr. Res.*, vol. 123, p. 105789, 2019.

[25] K. A. Erk and B. Bose, “Using Polymer Science To Improve Concrete: Superabsorbent Polymer Hydrogels in Highly Alkaline Environments,” in *Gels and Other Soft Amorphous Solids*, American Chemical Society, 2018, pp. 333–356. doi: 10.1021/bk-2018-1296.ch017.

[26] C. Schröfl, V. Mechtcherine, and M. Gorges, “Relation between the molecular structure and the efficiency of superabsorbent polymers (SAP) as concrete admixture to mitigate autogenous shrinkage,” *Cem. Concr. Res.*, vol. 42, no. 6, pp. 865–873, 2012.

[27] L. Montanari, P. Suraneni, M. T. Chang, C. Villani, and J. Weiss, “Absorption and Desorption of Superabsorbent Polymers for Use in Internally Cured Concrete,” *Adv. Civ. Eng. Mater.*, vol. 7, no. 4, pp. 547–566, 2018.

[28] J. Siramanont, W. Vichit-Vadakan, and W. Siriwatwechakul, “The Impact of SAP Structure on the Effectiveness of Internal Curing,” in *International RILEM conference on Use of superabsorbent polymers and other new additives in concrete*, pp. 243–252, 2010.

[29] C. R. Davis, B. Bose, A. Alcaraz, C. J. Martinez, and K. A. Erk, “Altering the Crosslinking Density of Polyacrylamide Hydrogels to Increase Swelling Capacity and Promote Calcium Hydroxide Growth in Cement Voids,” in *Third International RILEM Conference on the Application of Superabsorbent Polymers and Other New Admixtures Towards Smart Concrete*, 2019. doi: 10.1007/978-3-030-33342-3_3

[30] K. Farzanian and A. Ghahremaninezhad, “Desorption of superabsorbent hydrogels with varied chemical compositions in cementitious materials,” *Mater. Struct.*, vol. 51, no. 3, pp. 1–15, 2018.

[31] K. Farzanian and A. Ghahremaninezhad, “On the Effect of Chemical Composition on the Desorption of Superabsorbent Hydrogels in Contact with a Porous Cementitious Material,” *Gels*, vol. 4, no. 3 70, pp. 1–13, 2018.

[32] O. A. Mohamed and O. F. Najm, “Compressive strength and stability of sustainable self-consolidating concrete containing fly ash, silica fume, and GGBS,” *Front. Struct. Civ. Eng.*, vol. 11, no. 4, pp. 406–411, 2017.

[33] W. Aquino, D. A. Lange, and J. Olek, “The influence of metakaolin and silica fume on the chemistry of alkali–silica reaction products,” *Cem. Concr. Compos.*, vol. 23, no. 6, pp. 485–493, 2001.

[34] L. P. Singh, S. R. Karade, S. K. Bhattacharyya, M. M. Yousuf, and S. Ahalawat, “Beneficial role of nanosilica in cement based materials – A review,” *Constr. Build. Mater.*, vol. 47, pp. 1069–1077, 2013.

[35] L. Senff, J. A. Labrincha, V. M. Ferreira, D. Hotza, and W. L. Repette, “Effect of nano-silica on rheology and fresh properties of cement pastes and mortars,” *Constr. Build. Mater.*, vol. 23, no. 7, pp. 2487–2491, 2009.

[36] J. Björnström, A. Martinelli, A. Matic, L. Börjesson, and I. Panas, “Accelerating effects of colloidal nano-silica for beneficial calcium–silicate–hydrate formation in cement,” *Chem. Phys. Lett.*, vol. 392, no. 1–3, pp. 242–248, 2004.

[37] B.W. Jo, C.H. Kim, G. Tae, and J.B. Park, “Characteristics of cement mortar with nano-SiO2 particles,” *Constr. Build. Mater.*, vol. 21, no. 6, pp. 1351–1355, 2007.

[38] H. Biricik and N. Sarier, “Comparative study of the characteristics of nano silica - , silica fume - and fly ash - incorporated cement mortars,” *Mater. Res.*, vol. 17, no. 3, pp. 570–582, 2014.

[39] R. Merget *et al.*, “Health hazards due to the inhalation of amorphous silica,” *Arch. Toxicol.*, vol. 75, no. 11–12, pp. 625–634, 2002.

[40] L. B. Agostinho, de C. P. Alexandre, E. F. da Silva, and R. D. Toledo Filho, “Rheological study of Portland cement pastes modified with superabsorbent polymer and nanosilica,” *J. Build. Eng.*, vol. 34, p. 102024, 2021.
[41] A. Pourjavadi, S. M. Fakoorpoor, P. Hosseini, and A. Khaloo, “Interactions between superabsorbent polymers and cement-based composites incorporating colloidal silica nanoparticles,” *Cem. Concr. Compos.*, vol. 37, pp. 196–204, 2013.
[42] A. Pourjavadi, S. M. Fakoorpoor, A. Khaloo, and P. Hosseini, “Improving the performance of cement-based composites containing superabsorbent polymers by utilization of nano-SiO2 particles,” *Mater. Des.*, vol. 42, no. 2012, pp. 94–101, 2012.
[43] T. A. Cunha, L. B. Agostinho, and E. F. Silva, “Application of Nano-silica Particles to Improve the Mechanical Properties of High Performance Concrete Containing Superabsorbent Polymers,” in *3rd International Conference on the Application of Superabsorbent Polymers (SAP) and Other New Admixtures Towards Smart Concrete.*, vol. 24, Boshoff W., Combrinck R., Mechtcherine V., and Wyrzykowski M., Eds. Springer Cham, pp. 211–221, 2020.
[44] T. A. Cunha, P. Francinete, M. A. Manzano, L. A. Aidar, J. G. Borges, and E. F. Silva, “Determination of time zero in high strength concrete containing superabsorbent polymer and nano-silica,” *J. Build. Pathol. Rehabil.*, vol. 1, no. 1, pp. 1–12, 2016.
[45] G. Lefever *et al.*, “Combined use of superabsorbent polymers and nanosilica for reduction of restrained shrinkage and strength compensation in cementitious mortars,” *Constr. Build. Mater.*, vol. 251, p. 118966, 2020.
[46] G. Lefever, D. Snoeck, D. G. Aggelis, N. De Belie, S. Van Vlierberghe, and D. Van Hemelrijck, “Evaluation of the self-healing ability of mortar mixtures containing superabsorbent polymers and nanosilica,” *Materials (Basel).*, vol. 13, no. 2, 2020.
[47] G. Lefever *et al.*, “The Influence of Superabsorbent Polymers and Nanosilica on the Hydration Process and Microstructure of Cementitious Mixtures,” *Materials (Basel).*, vol. 13, no. 22, p. 5194, 2020.
[48] G. Olivier, R. Combrinck, M. Kayondo, and W. P. Boshoff, “Combined effect of nano-silica, super absorbent polymers, and synthetic fibres on plastic shrinkage cracking in concrete,” *Constr. Build. Mater.*, vol. 192, pp. 85–98, 2018.
[49] J. Justs, M. Wyrzykowski, D. Bajare, and P. Lura, “Internal curing by superabsorbent polymers in ultra-high

performance concrete," *Cem. Concr. Res.*, vol. 76, pp. 82–90, 2015.

[50] M. J. Krafcik, B. Bose, and K. A. Erk, "Synthesis and Characterization of Polymer-Silica Composite Hydrogel Particles and Influence of Hydrogel Composition on Cement Paste Microstructure," *Adv. Civ. Eng. Mater.*, vol. 7, no. 4, pp. 590–613, 2018. doi: 10.1520/ACEM20170144.

[51] K. A. Erk, "Cementitious Mixtures, Compositions for Use in Cementitious Mixtures, and Methods of Producing Cementitious Mixtures," U.S. Letters Patent 10,081,573. Issued on Sep 25, 2019.

[52] M. Rubinstein and R. H. Colby, *Polymer physics*, 1st ed. Oxford University Press, 2003.

[53] V. Mechtcherine *et al.*, "Testing superabsorbent polymer (SAP) sorption properties prior to implementation in concrete: results of a RILEM Round-Robin Test," *Mater. Struct.*, vol. 51, no. 28, pp. 1–16, 2018.

[54] D. Snoeck, C. Schröfl, and V. Mechtcherine, "Recommendation of RILEM TC 260-RSC: testing sorption by superabsorbent polymers (SAP) prior to implementation in cement-based materials," *Mater. Struct. Constr.*, vol. 51, no. 5, pp. 1–7, 2018.

[55] C. Schröfl, D. Snoeck, and V. Mechtcherine, "A review of characterisation methods for superabsorbent polymer (SAP) samples to be used in cement-based construction materials: report of the RILEM TC 260-RSC," *Mater. Struct.*, vol. 50, no. 197, pp. 1–19, 2017.

[56] W. Siriwatwechakul, J. Siramanont, and W. Vichit-Vadakan, "Behavior of Superabsorbent Polymers in Calcium- and Sodium-Rich Solutions," *J. Mater. Civ. Eng.*, vol. 24, no. 8, pp. 976–980, 2012.

[57] M. Wyrzykowski, A. Assmann, C. Hesse, and P. Lura, "Microstructure development and autogenous shrinkage of mortars with C-S-H seeding and internal curing," *Cem. Concr. Res.*, vol. 129, p. 105967, 2020.

[58] C. R. Davis, S. L. Kelly, and K. A. Erk, "Comparing laser diffraction and optical microscopy for characterizing superabsorbent polymer particle morphology, size, and swelling capacity," *J. Appl. Polym. Sci.*, vol. 135, no. 14, pp. 1–10, 2018. doi:10.1002/app.46055.

[59] M. T. Hasholt and O. M. Jensen, "Chloride migration in concrete with superabsorbent polymers," *Cem. Concr. Compos.*, vol. 55, pp. 290–297, 2015.

[60] Y. Wehbe and A. Ghahremaninezhad, "Combined effect of shrinkage reducing admixtures (SRA) and superabsorbent polymers (SAP) on the autogenous shrinkage, hydration and

properties of cementitious materials," *Constr. Build. Mater.*, vol. 138, pp. 151–162, 2017.
[61] K. Farzanian, K. Pimenta Teixeira, I. Perdigão Rocha, L. De Sa Carneiro, and A. Ghahremaninezhad, "The mechanical strength, degree of hydration, and electrical resistivity of cement pastes modified with superabsorbent polymers," *Constr. Build. Mater.*, vol. 109, pp. 156–165, 2016.
[62] R. Spragg, C. Villani, K. Snyder, D. Bentz, J. W. Bullard, and J. Weiss, "Factors that Influence Electrical Resistivity Measurements in Cementitious Systems," *Transp. Res. Rec. J. Transp. Res. Board*, vol. 2342, no. 1, pp. 90–98, 2013.
[63] K. Arroudj, A. Zenati, M. N. Oudjit, A. Bali, and A. Tagnit-Hamou, "Reactivity of Fine Quartz in Presence of Silica Fume and Slag," *Engineering*, vol. 3, pp. 569–576, 2011.
[64] J. Chisholm, "Comparison of quartz standards for X-ray diffraction analysis: HSE A9950 (Sikron F600) and NIST SRM 1878," *Ann. Occup. Hyg.*, vol. 49, no. 4, pp. 351–358, 2005.
[65] S. H. Behrens and D. G. Grier, "The Charge of Glass and Silica Surfaces," *J. Chem. Phys.*, vol. 115, pp. 6716–6721, 2001.
[66] J. Jiang, G. Oberdörster, and P. Biswas, "Characterization of size, surface charge, and agglomeration state of nanoparticle dispersions for toxicological studies," *J. Nanoparticle Res.*, vol. 11, no. 1, pp. 77–89, 2009.
[67] J. Yang, S. Meng, L. Xu, and E. G. Wang, "Water adsorption on hydroxylated silica surfaces studied using the density functional theory," *Phys. Rev. B*, vol. 71, no. 3, p. 035413, 2005.
[68] E. Asenath-Smith, H. Li, E. C. Keene, Z. W. Seh, and L. A. Estroff, "Crystal growth of calcium carbonate in hydrogels as a model of biomineralization," *Adv. Funct. Mater.*, vol. 22, no. 14, pp. 2891–2914, 2012.
[69] F. Nindiyasari, L. Fernández-Díaz, E. Griesshaber, J. M. Astilleros, N. Sánchez-Pastor, and W. W. Schmahl, "Influence of gelatin hydrogel porosity on the crystallization of CaCO 3," *Cryst. Growth Des.*, vol. 14, no. 4, pp. 1531–1542, 2014.
[70] J. A. Lopez-Berganza, S. Chen, and R. M. Espinosa-Marzal, "Tailoring Calcite Growth through an Amorphous Precursor in a Hydrogel Environment," *Cryst. Growth Des.*, vol. 19, no. 6, pp. 3192–3205, 2019.
[71] M. K. Jo, Y. Oh, H. J. Kim, H. L. Kim, and S. H. Yang, "Diffusion-Controlled Crystallization of Calcium Carbonate in a Hydrogel," *Cryst. Growth Des.*, vol. 20, no. 2, pp. 560–567, 2020.

[72] K. Farzanian and A. Ghahremaninezhad, “On the Interaction between Superabsorbent Hydrogels and Blended Mixtures with Supplementary Cementitious Materials,” *Adv. Civ. Eng. Mater.*, vol. 7, no. 4, pp. 567–589, 2018.
[73] M. Berra, F. Carassiti, T. Mangialardi, A. E. Paolini, and M. Sebastiani, “Effects of nanosilica addition on workability and compressive strength of Portland cement pastes,” *Constr. Build. Mater.*, vol. 35, pp. 666–675, 2012.
[74] D. Snoeck *et al.*, “The effects of superabsorbent polymers on the microstructure of cementitious materials studied by means of sorption experiments,” *Cem. Concr. Res.*, vol. 77, pp. 26–35, 2015.
[75] S. L. Kelly, M. J. Krafcik, and K. A. Erk, “Synthesis and Characterization of Superabsorbent Polymer Hydrogels Used as Internal Curing Agents in High-Performance Concrete : Impact of Particle Shape on Mortar Compressive Strength,” in *International Congress on Polymers in Concrete (ICPIC): Polymers for Resilient and Sustainable Concrete Infrastructure*, M. M. R. Taha, Ed. Springer International Publishing AG, pp. 91–97, 2018. doi: 10.1007/978-3-319-78175-4_9.

Article

Microstructural Refinement of Cement Paste Internally Cured by Polyacrylamide Composite Hydrogel Particles Containing Silica Fume and Nanosilica

Baishakhi Bose, Cole R. Davis and Kendra A. Erk*
School of Materials Engineering, Purdue University, West Lafayette, IN 47907 USA
*Correspondence: erk@purdue.edu, 765-494-4118

Supplemental Material

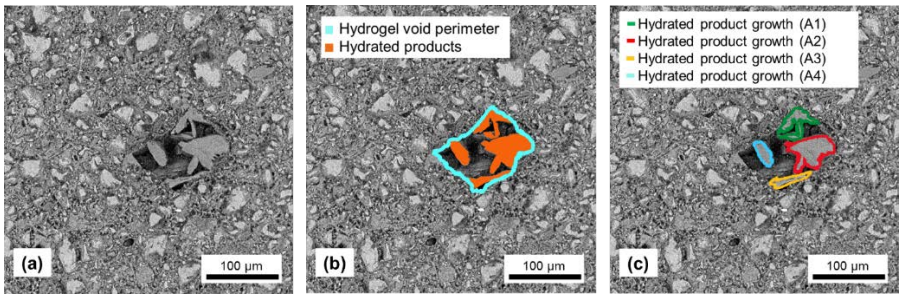

Figure S1: Calculation of area fraction of hydrated product growth in hydrogel-related void using ImageJ. (a) A deswollen hydrogel void. (b) The perimeter of the void is marked to find the total area of the void and the shaded regions shows the areas where hydrated products have deposited/grown. (c) Each area with product growth is separately marked off at the perimeter and the area within is calculated, totaled and divided by the total area of the void from (b) to obtain the area fraction of the hydrated product growth in this hydrogel particle void. 30 such hydrogel particle voids were analyzed for each type of internally cured cement paste composition.

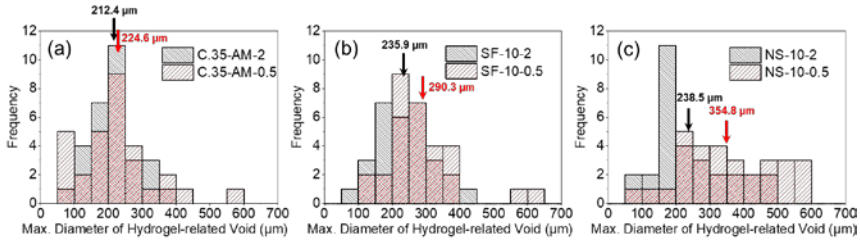

Figure S2: Maximum Diameter of Hydrogel-related voids as a function of cement paste composition. 3 days aged cement paste internally cured with (a) C.35-AM-2 and C.35-AM-0.5, (b) SF-10-2 and SF-10-0.5, (c) NS-10-2 and NS-10-0.5 were used for analysis and plotting the histogram. Arrows show the average maximum diameter of 30 imaged voids for that particular sample.

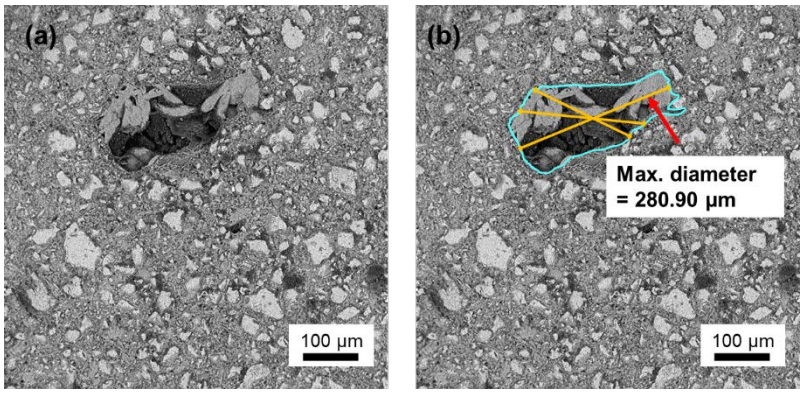

Figure S3: (a) Micrograph of cement paste with the hydrogel-related voids contained significant growth of hydrated product, obscuring the original dimensions of the swollen hydrogel particles. (b) Visible edges of the hydrogel-related voids were marked off and the diameter in several directions were measured to obtain the maximum diameter.

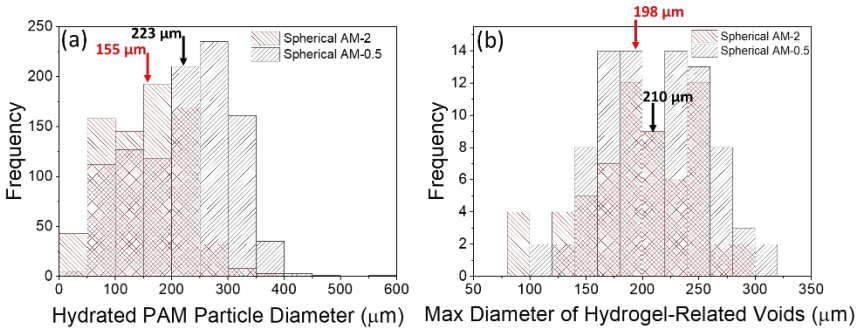

Figure S4: (a) Hydrogel particle diameter of spherical PAM in hydrated state measured using Optical microscopy (OM) paired with ImageJ. (b) Maximum diameter of hydrogel-related voids in cement paste measured using scanning electron microscopy (SEM) and ImageJ. Reducing the crosslinker amount allows for more water absorption and thus, a larger hydrated particle size was measured. Although hydrated PAM particles containing 0.5% crosslinker amount were larger, the difference in their respective void size in cement paste micrograph were not statistically significant with a confidence of 95% ($p = 0.061$). More details in Davis *et al.*, [26].

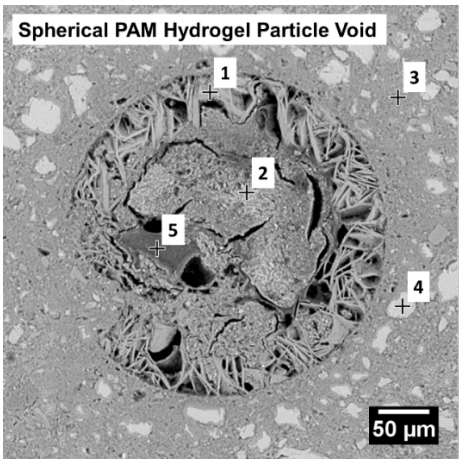

	Atomic Percent in Each Spot				
Element	1	2	3	4	5
O	68.3	71.6	69.3	62.7	72.2
Ca	27.2	11.5	18.4	25.1	9.5
Si	1.8	4.1	4.7	8.5	4.4
K	0.5	6.8	0.5	0.2	2.4
Na	0.9	1.4	0	0.6	5.3
Mg	0.7	0.6	1.4	1.4	0.5
Al	0.6	1	3.5	1.4	0.9
S	0	3.1	1.3	0	0
Fe	0	0	0.8	0	0
N	0	0	0	0	4.8

Figure S5: A SEM micrograph of cement paste internally cured with spherical shaped PAM along with the energy dispersive X-ray spectroscopy (EDS) done for elemental composition analysis. From the morphology and the elemental composition analysis, the product growth inside the hydrogel void is considered to be CH with some C-S-H intermixed. More details in Davis *et al.*, [26].

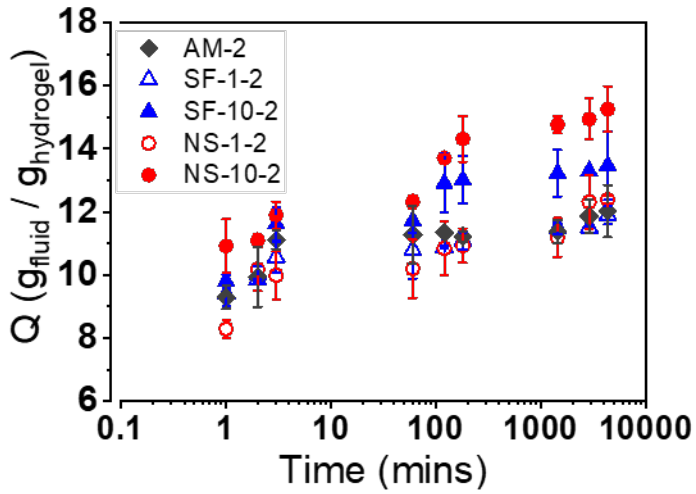

Figure S6: Swelling capacity of hydrogel particle samples as a function of immersion time in pore solution from 1 minute to 3 days.